4

Silicate & Opaque Mineral Petrography

4.1. Petrographic Descriptions of the Main Rock Types

Nebo Granite

The Nebo Granite of the study area is dominated by a mineral assemblage of perthite (K-feldspar) (65 %), quartz (35 %), biotite (2 %), plagioclase (An_{10}) (< 1 %), and hornblende (< 1 %), with minor accessory phases (1 %) including magnetite, zircon, sericite, fluorite, chlorite and occasional pyrite (Plate 4.1 (a)). Coarse varieties have a normal phaneritic, isogranular texture with holocrystalline mesostasis of all phases. The granite may exhibit slight granophyric texture in places. The coarse-grained Bobbejaankop granites are mafic-poor relative to the Nebo granites but resemble Nebo assemblages in most other respects. K-feldspar grains in these rocks are usually 10 mm or less in size and quartz grains 2-5 mm in size.

As discussed previously, the plagioclase and hornblende contents decrease upwards in the granitic sheet, and inversely, the perthite and quartz contents increase upwards. The Klipkloof granite maintains a similar mineral assemblage throughout the granite sheet, except for hornblende, which is either scarce or absent (Kleeman & Twist, 1989) and is characterised by fine plagioclase needles (Plate 4.1 (b)).

Idiomorphic plagioclase is most common in the basal portions of the sheet, and apparently formed before the quartz and perthite (Kleeman & Twist, 1989). It is presumed that the granites of the study area are too high in the stratigraphy to exhibit such features. In the middle portion of the sheet the co-crystallization of

plagioclase, quartz and perthite appears to have prevailed (Plate 4.1 (c)-(d)). In the uppermost portions of the granite sheet and in the contact facies of the granites, subhedral and anhedral quartz is set in mat of subhedral to anhedral perthite, with interstitial femic clusters dominated by biotite. Any plagioclase precipitated at this time tends to be interstitial and was probably crystallized last.

The evolving textural variation of the plagioclase component of the Nebo granite can be represented in terms of hypersolvus-subsolvus crystallisation. Subsolvus granites are characterised by the occurrence of discrete albite plagioclase and (non-perthitic) K-feldspar phases, whereas hypersolvus granites are characterised by the absence of discrete albitic plagioclase crystals, with albite occurring only as a component of perthite. The formation of this perthitic K-feldspar is possible under dry, near-surface environments (Martin & Bonin, 1976). According to Kleeman & Twist (1989), the Nebo granites should therefore exhibit a subsolvus character in the lower portions of the granite sheet, and hypersolvus character in the upper portions.

Intrusive Klipkloof variety granites contain discrete phases of both albite and K-feldspar, and would therefore be regarded as subsolvus; implying an added aqueous component, possibly meteoric-derived (Freeman, 1998). Porphyritic contact facies granites, occurring between Nebo granite and Klipkloof granite exhibits intermediate characteristics with perthite occurring in a subsolvus matrix (Freeman, 1998).

The K-feldspars have been increasingly deuterically altered and ferro-oxide-stained higher in the granite sheet, due to the liberation of ferric iron as hematite from the perthite lattice, a feature that accounts for the increased reddening upwards. They have also been sericitised and chloritised in places, principally due to mineralising fluids. The K-feldspar grains of the Nebo granites tend to be between 1-2 mm in size on average, though smaller grains are common and may coarsen to 10 mm or less (Plates 4.1 (e)-(f)). They occur generally as subrounded to irregularly-shaped grains. The majority of feldspars are orthoclase with a

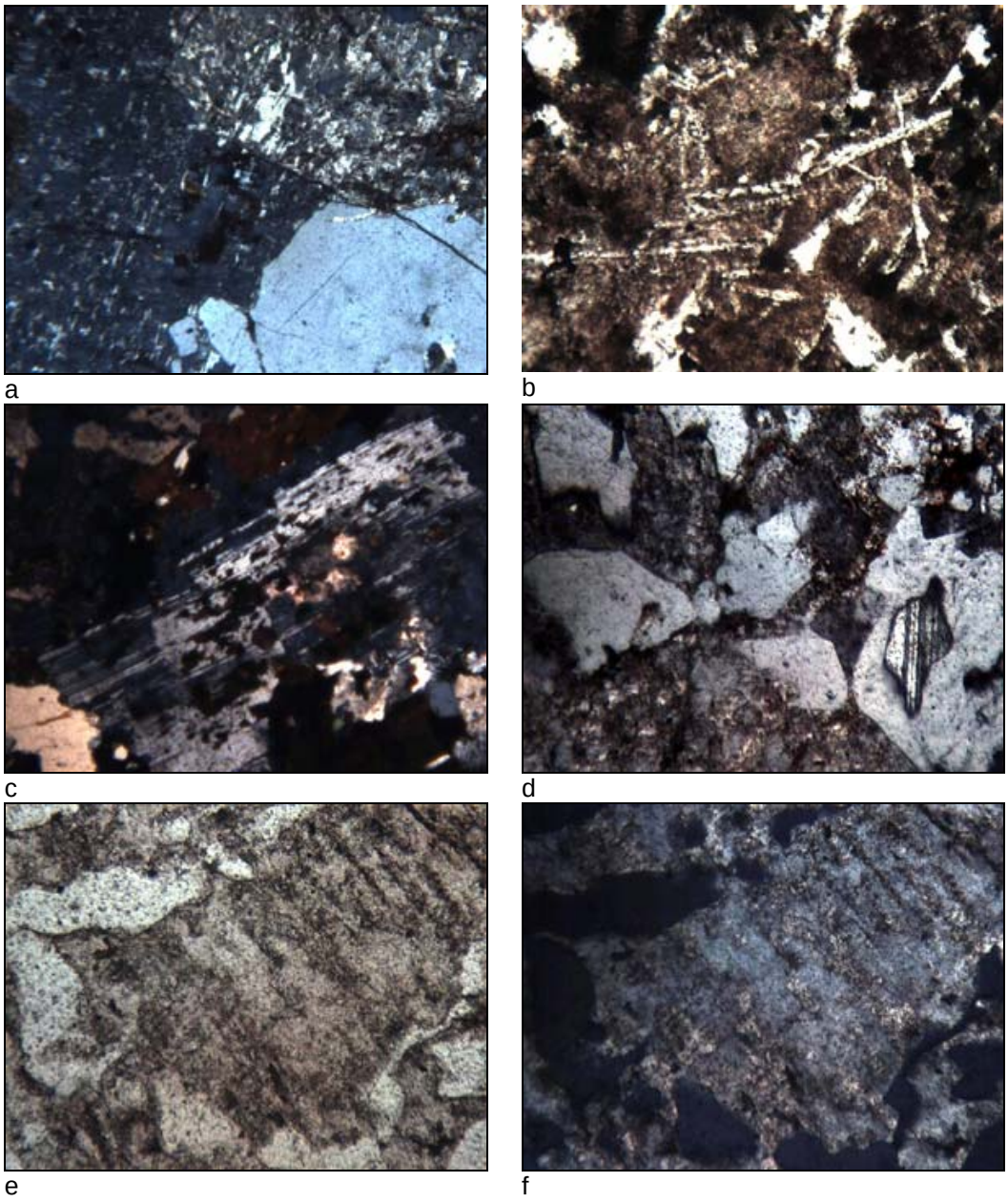

Plate 4.1. a) Typical hypersolvus, perthitic granite comprising perthite and quartz. Accessory phases not visible in this photograph. Crossed polars x4; field of view is 2.75 mm wide; Photo ID: 11097-F. b) Typical subsolvus Klipkloof granite with plagioclase needles, indicative of super-cooling. Plane polars x10; field of view is 0.85 mm wide; Photo ID: 11212-B. c) Transsolvus granite as defined by the occurrence of both albite plagioclase and perthite. Crossed polars x4; field of view is 2.75 mm wide; Photo ID: 11103-H. d) Anhedral comagmatic perthite and quartz, with quartz completely enclosing an albite plagioclase grain. Crossed polars x10; field of view is 0.85 mm wide; Photo ID: 11193-G. e) Anhedral perthitic K-feldspar. Plane polars x10; field of view is 0.85 mm wide; Photo ID: 11194-C. f) Anhedral perthitic K-feldspar. Crossed polars x10; field of view is 0.85 mm wide; Photo ID: 11194-D.

perthitic overgrowth and damaged by speckled sericite replacement. Only minor amounts of albite have been identified.

Quartz grains of the Nebo granites tend to be between 0.5 and 1.5 mm in size on average and are subhedral to anhedral, and may be intergrown with the larger orthoclase grains. Quartz grains in the upper portions of the granite sheet often display an array of shapes and embayments due to corrosion, re-sorption or re-precipitation (Coetzee & Twist, 1989) during late- and post-magmatic processes (Plates 4.2 (a)-(b)).

Klipkloof granites exhibit hypovolcanic textures, which are generally sub-isogranular and granophyric in places. Mineral phases tend to be 0.5 mm in size or less with feldspar needles developed in places.

Hornblende and biotite are present in the Nebo granite as their Fe-rich end-members, ferro-edenite and annite, respectively (Kleeman & Twist, 1989). Both phases occur interstitial to the other rock-forming phases and are considered to be late in the crystallization sequence. They have both been extensively chloritised. Biotite commonly forms characteristic symplectic intergrowths with quartz (Plates 4.2 (c)-(d)). It varies in colour from pleochroic light yellow-brown to dark brown, and light green-brown to dark green. It typically tends to be between 0.5 and 1.0 mm in size on average. Mafic phases in the granites tend to occur as interstitial clots in close association with magnetite and other accessory phases.

Interstitial accessory phases of the Nebo granite include: zircon, fluorite, ilmenite, magnetite, pyrite and apatite (Plate 4.2 (e)); with other phases, as determined by scanning electron microscope (Kleeman & Twist, 1989), including: thorite, tourmaline, calcite, sphene, galena, sphalerite, arsenopyrite, chalcopyrite and molybedenite, monazite, muscovite, and rutile.

Primary magnetite grains tend to be between 0.05 to 0.5 mm and may be euhedral to anhedral. Secondary magnetite is associated with the final stages of the

paragenetic sequence where hematite, quartz and fluorite are more abundant (Freeman, 1988).

Sulphides and magnetite may occur along biotite cleavage planes and have been interpreted as subsolidus hydrothermal alteration products which are commonly closely associated with chloritised mafic constituents (Kleeman & Twist, 1989; Bailie, 1997) The intergrowth of biotite and hematite demonstrates the intimate relationship between potassium and iron metasomatism (Plate 4.2 (f)).

Although accessory phases such as magnetite, ilmenite, apatite, thorite and monazite may be found as inclusions within silicates, they are generally found interstitial to the other rock-forming constituents. These phases are early-formed magmatic minerals and their distribution may reflect large differences in surface tensions between accessories and the main crystallising silicates which may preferentially exclude the accessories until they become trapped in final pore spaces (Kleeman & Twist, 1989).

Rashoop Granophyres

The granophyre of the Bushveld is dominated by a mineral assemblage involving the symplectic intergrowth of K-feldspar and quartz in roughly equal proportions, with minor accessory phases (Plate 4.3 (a)-(b)). Nucleation sites for the granophyric texture may have been a euhedral K-feldspar phenocryst or may have no discernable nucleation point whatsoever. The texture, in general, is finer-grained closest to the nucleation point and coarsens as it radiates outwards. Optical continuity is maintained between like mineral phases, i.e. all K-feldspar grains will extinguish at the same angle, as will all quartz grains extinct at the same angle.

Minor accessory mineral components of the granophyre include subhedral and commonly skeletal biotite, anhedral to euhedral magnetite, chlorite, sphene, zircon, apatite, calcite and rare fluorite (Bailie, 1997; Gain & Twist, 1995).

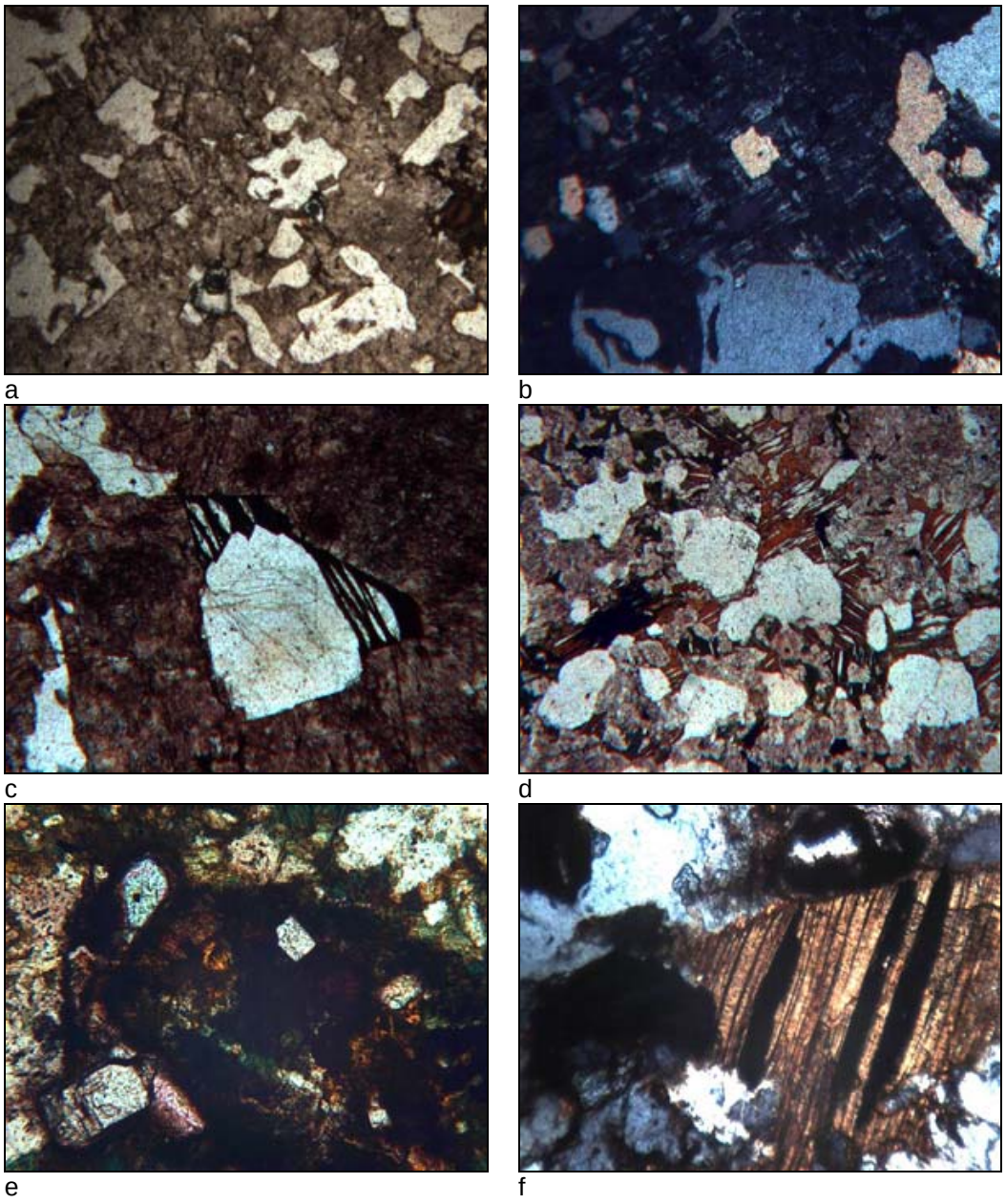

Plate 4.2. a) Embayed and resorbed quartz grains intergrown with K-feldspar. Plane polars x4; field of view is 2.75 mm wide; Photo ID: 11121-C. b) Embayed and resorbed quartz grains intergrown with K-feldspar. Crossed polars x4; field of view is 2.75 mm wide; Photo ID: 11049-M. c) Biotite-quartz symplectite. Plane polars x4; field of view is 2.75 mm wide; Photo ID: 11023-K. d) Biotite-quartz symplectite. Plane polars x4; field of view is 2.75 mm wide; Photo ID: 11034-A. e) Cluster of accessory phases including zircons, chloritised biotite, magnetite and other iron oxides. Crossed polars x20; field of view is 0.45 mm wide; Photo ID: 11067-L. f) Interstitial biotite with subsolidus hydrothermal magnetite developed along cleavage planes demonstrating the relationship between K- and Fe- metasomatism. Crossed polars x10; field of view is 0.85 mm wide; Photo ID: 11193-F.

Rooiberg Rhyolites, Pseudogranophyres and Agglomerates

The rhyolites of the Rooiberg Group are fine to very fine-grained (approximate grain size 0.05 mm or smaller), and comprise plagioclase feldspar, K-feldspar and quartz with minor very fine magnetite and hematite. The constituents tend to be anhedral to subhedral (Plate 4.4 (a)). The feldspars are commonly sericite and/or chlorite altered. Dispersed phenocrysts of altered feldspar, titanomagnetite, small needles of apatite and very rare augite may occur (Gain & Twist, 1995).

Pseudogranophyres are generated from Rooiberg rhyolites that have been recrystallised along the contact with the intruding granites. The texture is a combination of the granitic and granophyric textures, which tends to be most coarse towards the rhyolite-granite contact. Plate 4.3 (d) demonstrates such a relationship where the granophyric intergrowth of quartz and K-feldspar is nucleated from the side of a pre-existing K-feldspar grain. A variety of intergrowth textures may be observed in the pseudogranophyres including graphic, spotted, streaky, and donut graphic (Plates 4.3 (e)-(f) and Plate 4.4 (a)).

The agglomerate unit of the Rooiberg Group is generally dark brown in colour, but may also be green, beige and purplish brown. It is composed of a fine matrix, generally 0.05 mm or less in size, of completely sericitised and chloritised plagioclase and K-feldspar, chalcedonic quartz, and fine hematite (Plates 4.4 (b)-(c)). Fine needles in the groundmass composed entirely of alteration products, most prominently ferrohydroxides, may be indicative of supercooling of the agglomeratic unit (Plate 4.4 (d)). Fragments in the agglomerate are most commonly highly-altered, subhedral feldspar grains which are frequently completely obscured by the alteration products sericite and hematite (Plates 4.4 (e)-(f)). Other fragments are lithic in nature of rhyolite, granophyre and quartzo-feldspathic sedimentary rocks of the overlying Rooiberg. The fragments may be angular to sub-rounded and range in size from 10 cm to 0.5 mm or less.

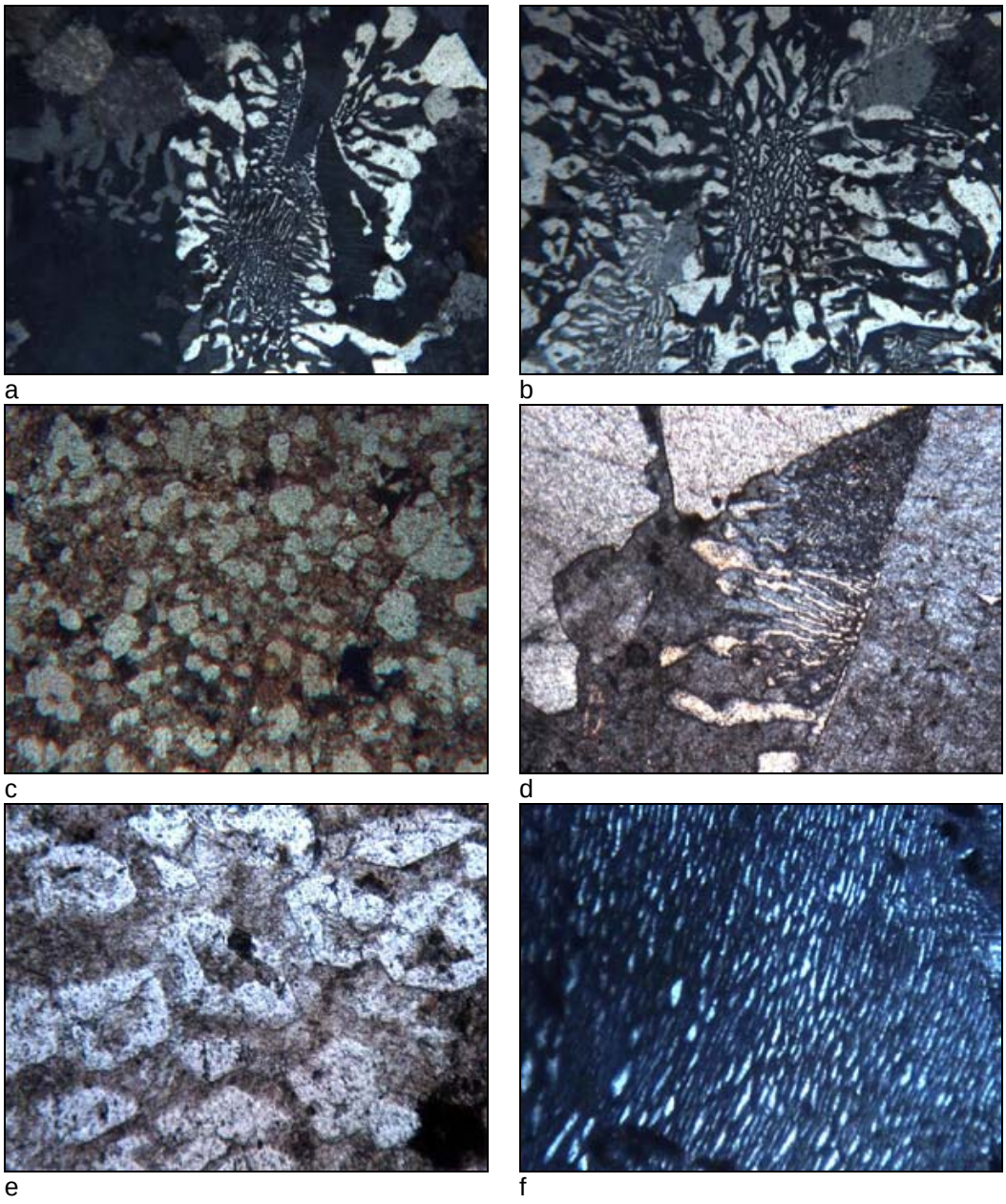

Plate 4.3. a) Granophyric texture of typical granophyre. Crossed polars x4; field of view is 2.75 mm wide; Photo ID: 11102-A. b) Granophyric texture with no discernible nucleation point Crossed polars x4; field of view is 2.75 mm wide; Photo ID: 11102-B. c) Typical massive Rooiberg rhyolite consisting of quartz, feldspar and minor biotite. Plane polars x4; field of view is 2.75 mm wide; Photo ID: 11049-J. d) Coarse pseudogranophyre from Elandslaagte 154JQ. Fine stringy quartz-feldspar symplectic intergrowth nucleating off the side of K-feldspar grain. Crossed polars x4; field of view is 2.75 mm wide; Photo ID: 11058-A. e) Donut graphic texture of pseudogranophyre. Plane polars x10; field of view is 0.85 mm wide; Photo ID: 11213-H. f) Streaky texture of pseudogranophyre. Crossed polars x4; field of view is 2.75 mm wide; Photo ID: 11213-I.

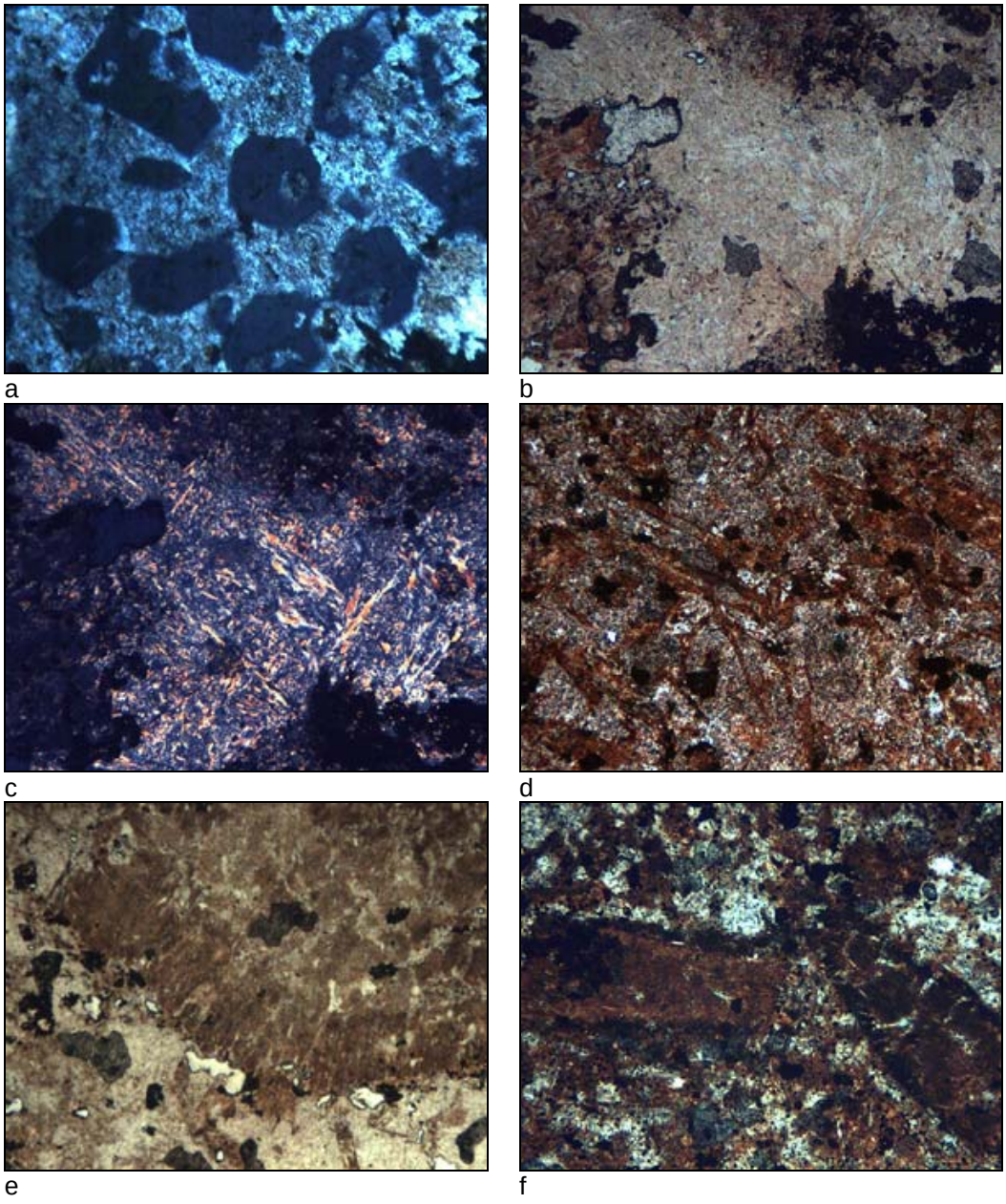

Plate 4.4. a) Spotted texture of pseudogranophyre. Crossed polars x10; field of view is 0.85 mm wide; Photo ID: 11213-E. b) Agglomerate groundmass composed of chalcedonic quartz and sericite. Plane polars x4; field of view is 2.75 mm wide; Photo ID: 11076-E. c) Agglomerate groundmass composed of chalcedonic quartz and sericite. Crossed polars x4; field of view is 2.75 mm wide; Photo ID: 11076-F. d) Fine needles, altered and obscured by ferrohydroxides, in agglomerate possibly indicative of supercooling. Plane polars x4; field of view is 2.75 mm wide; Photo ID: 11088-A. e) Angular fragment in agglomerate with relict faces of feldspar crystal; completely altered. Plane polars x4; field of view is 2.75 mm wide; Photo ID: 11076-A. f) Subhedral lathlike fragments in agglomerate, presumably feldspar crystals, completely obscured by hematite and other ferrohydroxides. Plane polars x10; field of view is 0.85 mm wide; Photo ID: 11076-G.

Quartzitic xenoliths

The quartzitic sedimentary xenoliths are composed almost entirely of annealed quartz grains that underwent recrystallisation, presumably during the intrusion of the granites such that virtually no pore space was retained. Grains are randomly oriented and are irregularly-shaped to rounded (Plates 4.5 (a)-(c)). Sericite, magnetite, hematite and other ferrohydroxides account for 1 % or less of the total rock and occur along grain boundaries and microfractures.

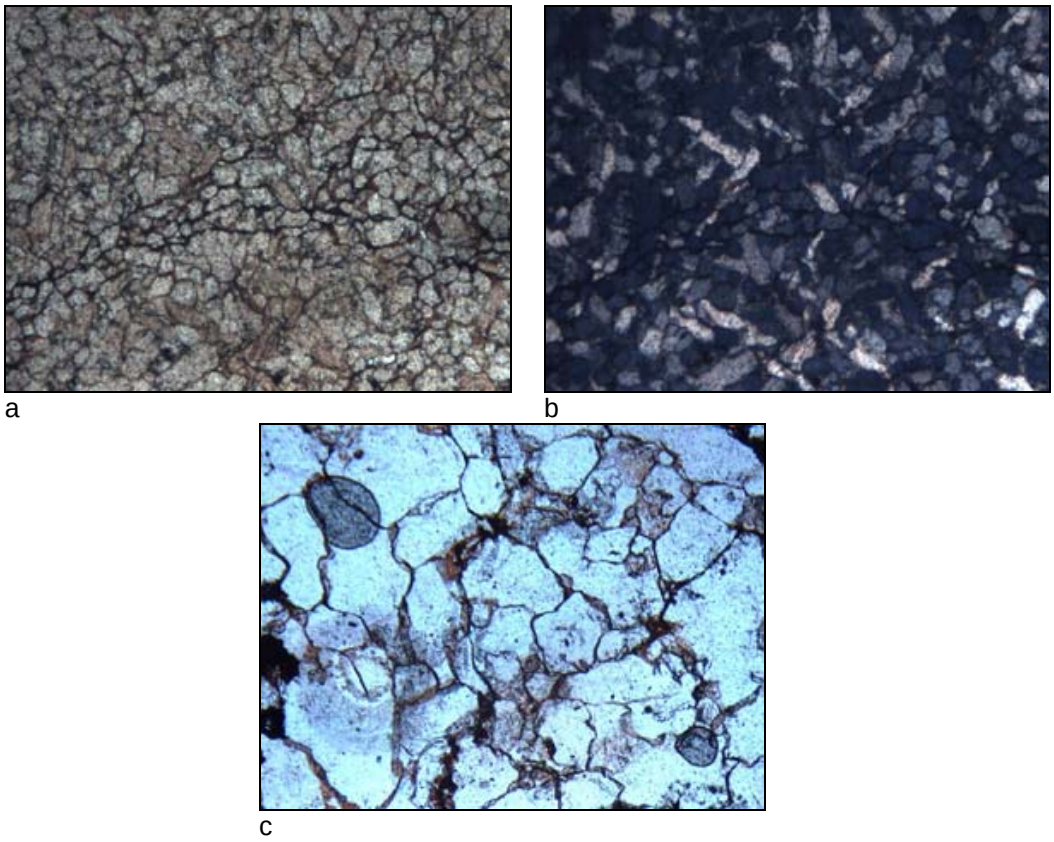

Plate 4.5. a) Quartzitic xenolith near granite roof principally composed of mosaic textured quartz, with iron oxides along grain boundaries and microfractures. Plane polars x4; field of view is 2.75 mm wide; Photo ID: 11072-A. b) Quartzitic xenolith near granite roof principally composed of mosaic textured quartz, with iron oxides along grain boundaries and microfractures. Crossed polars x4; field of view is 2.75 mm wide; Photo ID: 11072-B. c) Annealed quartz of sedimentary xenolith. Minor phases include sericite and iron oxides. Plane polars x4; field of view is 2.75 mm wide; Photo ID: 11150-A.

4.2. Petrographic Descriptions of the Mineralised and Ore Zone Rock Types

Ferroactinolite Britholite Rock

The high-temperature, primary mineral assemblage corresponding to many of the deposits in the district is postulated as being originally dominated by dark-green to black ferroactinolite with minor magnetite and britholite. In many deposits this assemblage occurs as radiating pneumatolytic growths along the sidewalls of fissures and breccias (Crocker *et al*., 1988). For instance, as with the Blokspruit mega-breccias, amphibole growth was permitted to fill most spaces to form a continuous mass.

The dark ferroactinolite occurs as high relief, bladed aggregates of thin lath-like crystals or in radiating crystals. Under plane polarised light it may be yellow-green to blue-green and demonstrates strong pleochroism from yellow-green to dark green (Plate 4.6 (a)); or in less mafic examples from colourless to light green to dark green (Plate 4.6 (b)). Few pristine examples exist in the area, the ferroactinolite pervadingly altered to chlorite, or pseudomorphed by silica and hematite (Plates 4.6 (c)-(e)). According to Crocker *et al*. (2001), it may also be altered to nontronite, a lime-green mineral of the smectite family commonly associated with ferroactinolite, although this has not been fully corroborated petrographically.

Britholite occurs as an important accessory phase and may constitute up to 5 % of the total volume of the assemblage in some instances. In thin section it forms massive, high relief grains that are yellowish brown in colour under plane polarised light (Plate 4.6 (f)). In altered samples, britholite is altered to red goethite (Crocker *et al*. 1988).

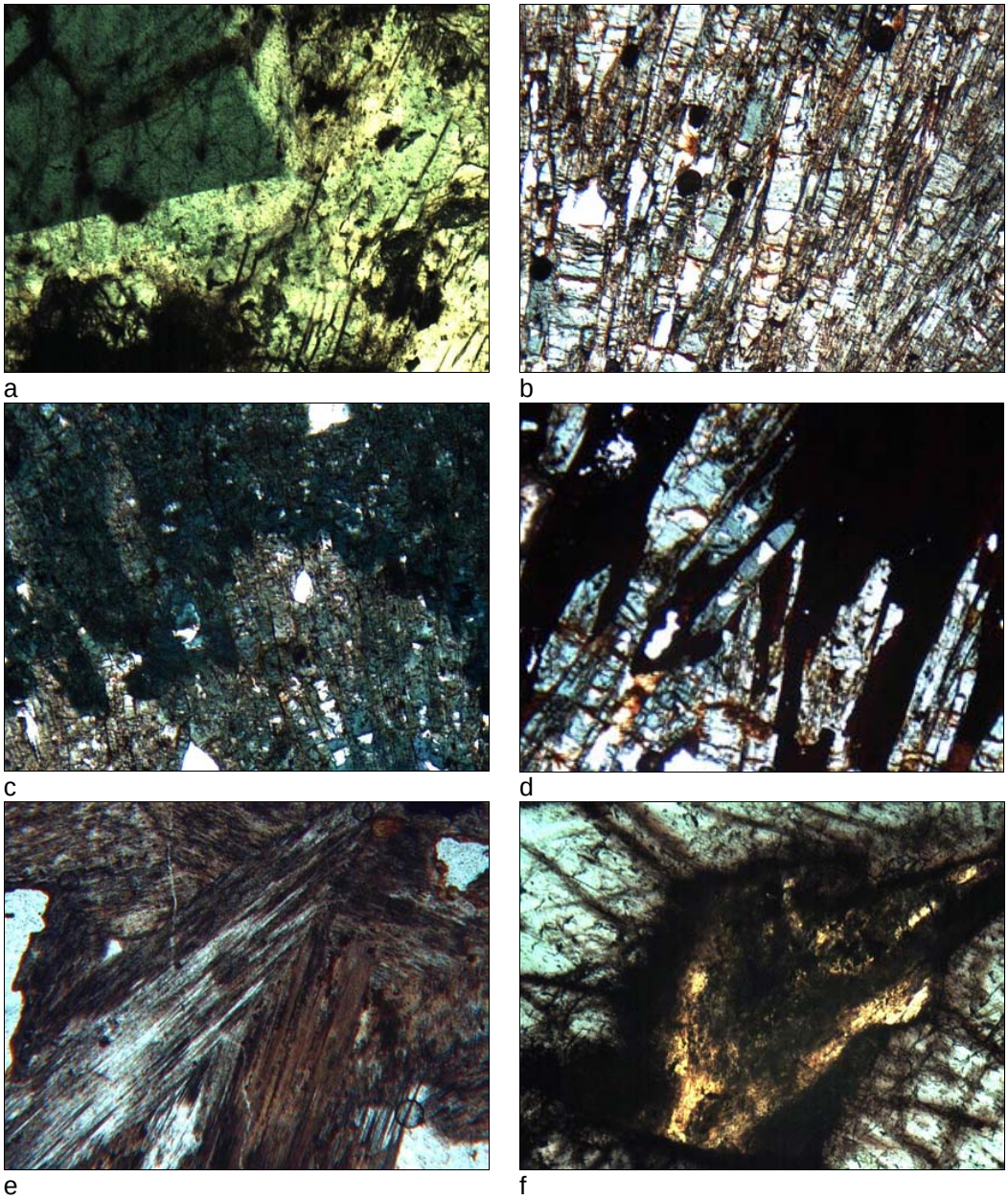

Plate 4.6. a) Fresh yellowish-green ferroactinolite. Plane polars x4; field of view is 2.75 mm wide; Photo ID: 11091-A. b) Colourless to pale green, unaltered actinolite with rounded oxide grains. The brownish phase along grain margins and in fractures may be nontronite. Plane polars x4; field of view is 2.75 mm wide; Photo ID: 11139-D. c) Pervasive chloritisation alteration front over actinolite. Plane polars x4; field of view is 2.75 mm wide; Photo ID: 11139-C. d) Hematite replacement of actinolite. Plane polars x4; field of view is 2.75 mm wide; Photo ID: 11139-F. e) Silica-hematite pseudomorph after actinolite. Plane polars x4; field of view is 2.75 mm wide; Photo ID: 11046-A. f) Yellowish brown Y-britholite. Plane polars x4; field of view is 2.75 mm wide; Photo ID: 11091-E.

Massive Iron Oxide-Quartz-Fluorite Assemblage

The mineralogy of IOCG systems is invariably characterised by abundant iron oxide minerals, dominated by hematite, magnetite or both. IOCG deposits are no longer considered to be charaterised by mutually exclusive hematite or magnetite, as may have once been presumed; Olympic Dam, for example, has been shown to have had an earlier magnetite episode to that of the development of ubiquitous hematite.

The source of abundant iron oxides located in fractures, veins, breccia fill and as massive pods is not certain. They may represent a late fluid fraction genetically related to the crystallising Bushveld granites, a hydrothermal fluid phase of a later intrusive event responsible for IOCG mineralisation, or a combination and superimposition of both of these ideas. These fractures and veins appear to follow consistent orientations, and it remains to be determined whether specific structural orientations correspond to distinct orogenic or intrusive events.

Petrographic investigations of the iron oxides have shown that they comprise an early magnetite phase, which may occur as euhedral crystals in quartz or fluorite, that is partially to wholly replaced by hematite (Plate 4.7 (a)). Although the magnetite may have contained minor amounts of early specular hematite, the principal development of hematite was the result of subsequent hydrothermal fluids. Plate 4.7 (b) shows the textural character of hydrothermal replacement of magnetite (Mt; grey) by hematite (Hm; light grey). The initial hematite replacement occurs especially along the grain boundaries of the magnetite and to a lesser extent may also occur along the octahedral crystallographic planes of the magnetite.

Hematite is, however, by far the more abundant iron oxide phase, and is most commonly massive and specularitic. Gossanous and supergene reniform and botryoidal forms are also observed. Specularitic ores may be very fine or coarse and flaky (Plate 4.7 (c)). It is associated with other iron oxides, hydrothermal

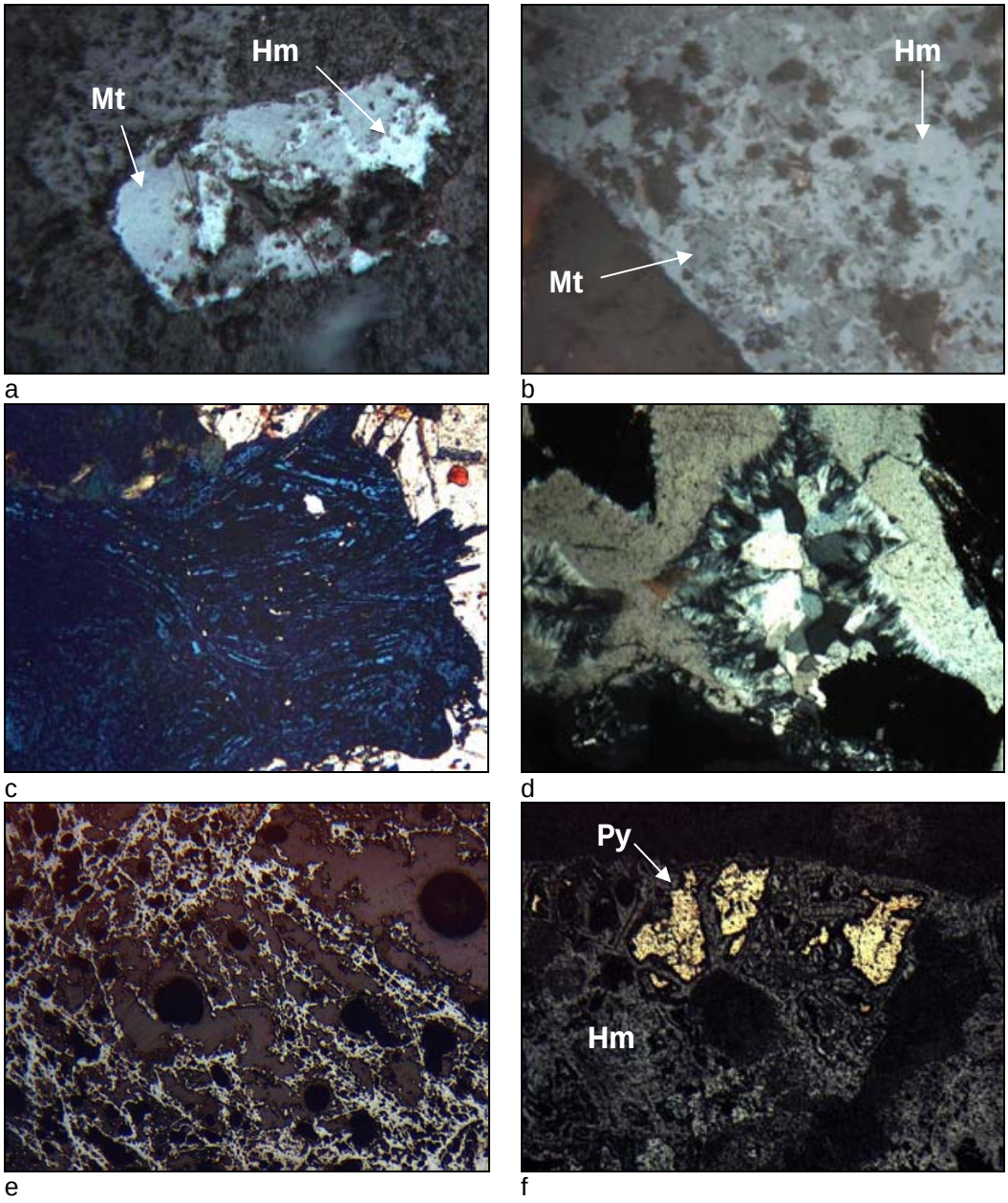

Plate 4.7. a) Euhedral magnetite in quartz partially oxidised to hematite. Mt=magnetite, Hm=hematite. Reflected light x50; field of view is 0.16 mm; Photo ID: 11194-N. b) Gossanous iron oxide of hematite with relict magnetite. Mt=magnetite, Hm=hematite. Reflected light x80; field of view is 0.10 mm; Photo ID: 11079-A. c) Specularite flakes from Ruigtepoort contact granite. Reflected light with Plane polars x4; field of view is 2.75 mm; Photo ID: 11067-Q. d) Quartz-hematite vein demonstrating multiple episodes of quartz growth. Plane polars x4; field of view is 2.75 mm; Photo ID: 11074-J. e) Hematite gossan. Rhombic forms may be indicative of primary siderite-magnetite in ore. Reflected light x4; field of view is 2.75 mm; Photo ID: 11055-A. f) Hematite gossan from Elandslaagte 154JQ with pyrite in cores of gossan lattice. Py=pyrite, Hm=hematite. Reflected light x4; field of view is 2.75 mm; Photo ID: 11074-E.

cryptocrystalline quartz (Plates 4.7 (d)) and minor fluorite and sulphides.

Hematite boxwork gossans of this assemblage are particularly common in ores dominated by magnetite-siderite-quartz with accessory fluorite and sulphides (Plates 4.7 (e)-(f) and Plate 4.8 (a)). Quartz is commonly recrystallised to form euhedral, prismatic crystals; often with multiple growth stages (Plate 4.8 (b)), which may terminate in triple junctions (Plate 4.8 (c)).

Two generations of fluorite have been noted with respect to mineralisation in the Bushveld granites (Crocker *et al*. 1988; Freeman, 1998); a primary, high-temperature fluorite that is green, purple or colourless and commonly has an octahedral habit (Plate 4.8 (d)). It is associated with fresh actinolite and hematite-quartz pseudomorphs after actinolite or with siderite-magnetite-quartz ores and the hematite gossans after these ores. A second generation of lower temperature, epithermal fluorite is found in veins within these deposits. This fluorite is predominantly purple in colour and has a botryoidal or cubic habit (Crocker *et al*. 1988). This generation of fluorite may be riddled with inclusions, may occur with bastnaesite and in some instances is slightly radioactive (Crocker *et al*. 1988).

Pseudomorphs of amphibole by hematite and quartz are well-documented in the district (Crocker *et al*., 1988, 2001). Petrographic sections of these pseudomorphs reveal that the replacement of the amphibole may be achieved by either hematite or quartz, with quartz being the more common substitute (Plates 4.8 (e)-(f)). In these instances, hematite occurs as inclusions or clots between the silicified needles (Plate 4.9 (a)).

The examples presented in Plates 4.9 (b)-(c) demonstrate examples of iron oxides occurring along perthite rims, within the grains and as veinlets and stringers cross-cutting the perthites. The sample in Plate 4.9 (b) corresponds to a site of mineralisation with intense chlorite-hematite alteration, and is likely unrelated to more regional scale albitisation effects. The sample in Plate 4.9 (c) was also

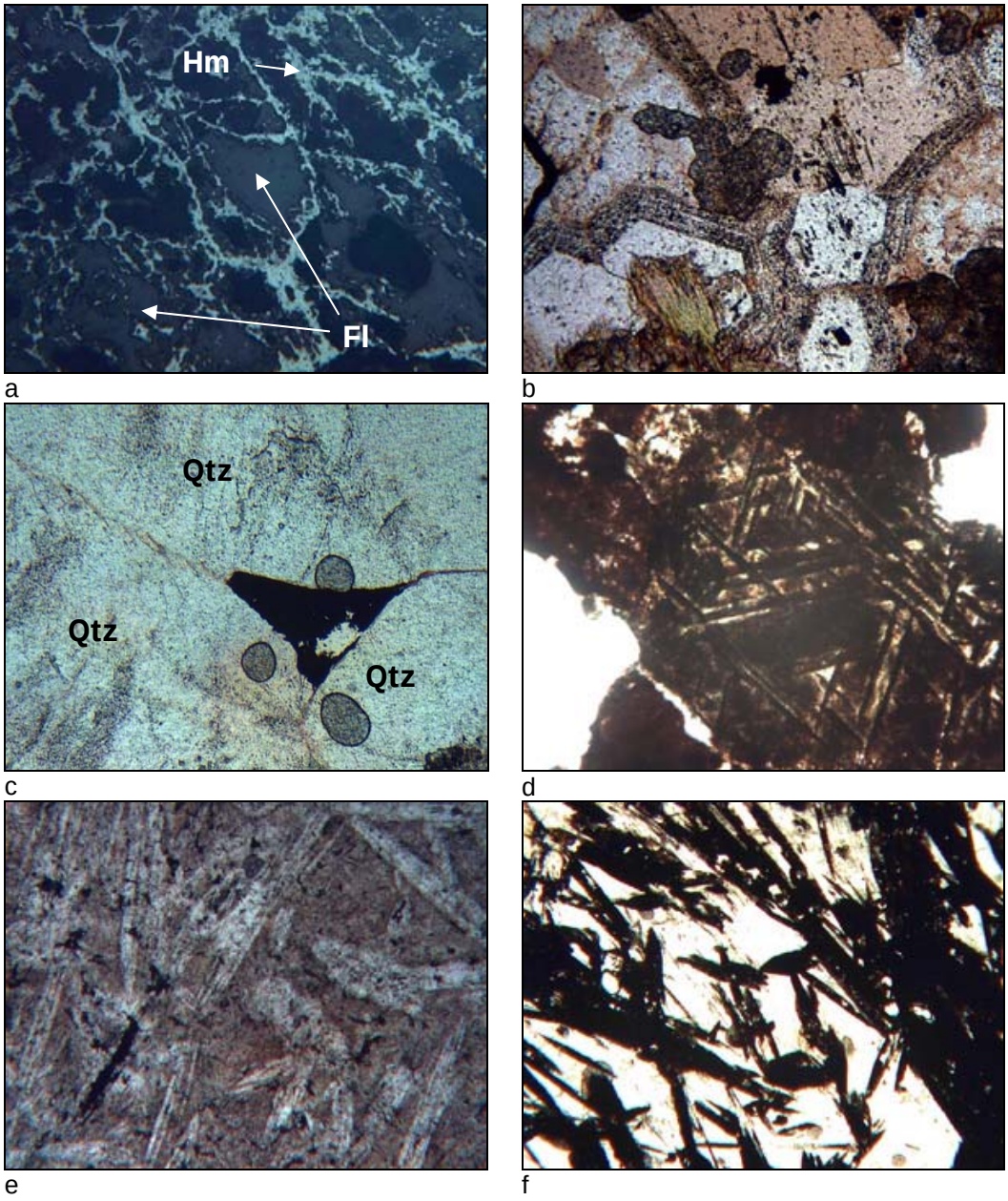

Plate 4.8. a) Hematite gossan. Primary fluorite still contained in some partitions. Hm=hematite, Fl=fluorite. Reflected light x20; field of view is 0.45 mm; Photo ID: 11055-A. b) Multiple growth phases of quartz associated to hematite ores. Plane polars x10; field of view is 0.85 mm; Photo ID: 11143-F. c) Quartz growth terminating in triple junction with hematite in final pore space. Qtz=quartz. Plane polars x4; field of view is 2.75 mm; Photo ID: 11055-H. d) Octahedral growth planes in high temperature fluorite. Plane polars x20; field of view is 0.45 mm; Photo ID: 11068-G. e) Pseudomorphed quartz after actinolite needles with fine inclusions of hematite. Matrix is quartz. Plane polars x4; field of view is 2.75 mm; Photo ID: 11037-F. f) Pseudomorphed hematite after actinolite with crystalline quartz matrix. Plane polars x4; field of view is 2.75 mm; Photo ID: 11037-C.

derived from a site of mineralisation and iron oxide veining is probably related to hydrothermal mechanical fracturing.

Zones of intense hydrothermal activity are marked by the distribution of hematite-filled breccias, as commonly noted at several mineral occurrences in the area. The breccia fill is commonly dominated by hematite but may also be composed of quartz and fluorite (Plate 4.9 (d)).

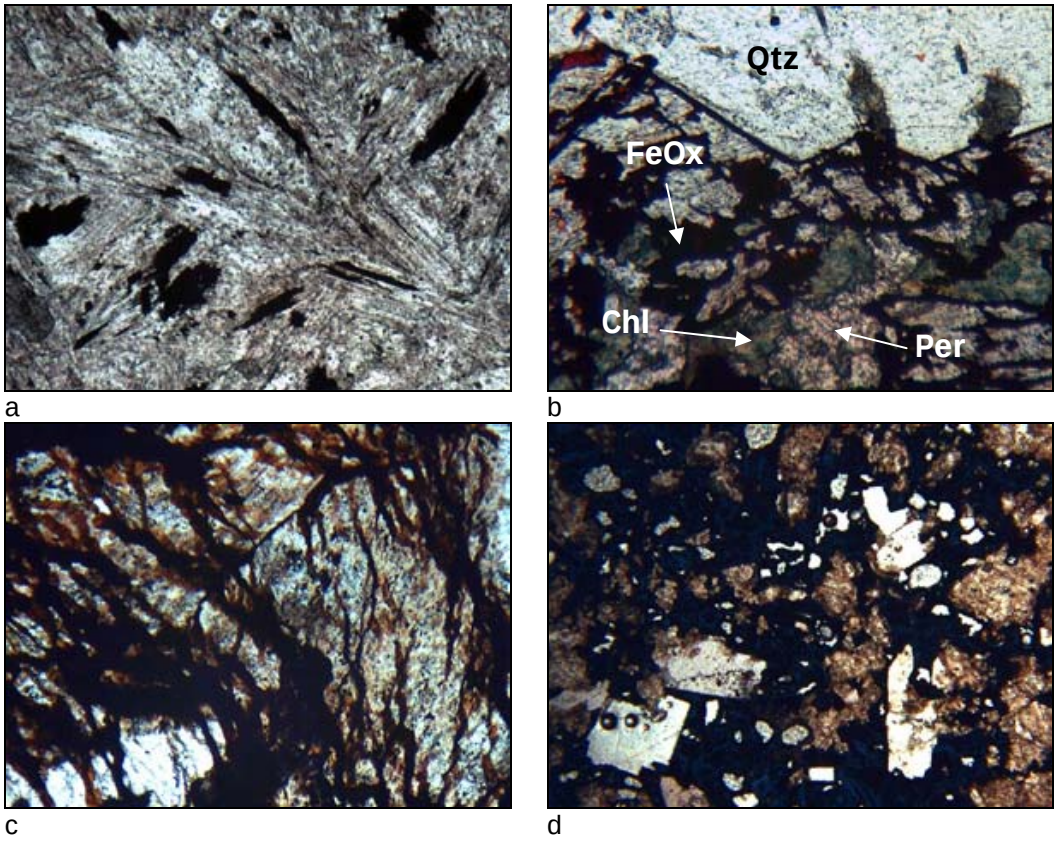

Plate 4.9. a) Pseudomorphed quartz after actinolite needles with larger aggregates of hematite. Plane polars x4; field of view is 2.75 mm; Photo ID: 11017-F. b) Chloritised granite with iron oxides developed within perthite and along grain boundaries. Plane polars x10; field of view is 0.85 mm; Photo ID: 11008-P. c) Iron oxides occurring as veins and stringers in actinolite rock. Plane polars x4; field of view is 2.75 mm; Photo ID: 11056-A. d) Granite breccia with hematite fill. Plane polars x4; field of view is 2.75 mm; Photo ID: 11149-B.

Chlorite-Fluorite-Sulphide Ore

Chlorite-dominated assemblages are found to be related to many of the mineralised deposits in the area. It is postulated that this is in direct correlation to the formation of actinolite in the ore zones and represents a subsequent alteration of amphibole to chlorite. Low-temperature chloritisation of the immediate country rocks is also observed which may represent a paragenetic retrograde alteration series as the system cooled.

The mineralogy of the ore zone is dominated by Fe-rich chlorite, commonly thuringite (Crocker *et al*., 2001), with fluorite, hematite, specularite, goethite and limonite with minor quartz and sulphides (Plate 4.10 (a)). The chlorite normally forms a fine netted mass, although radiating needles after actinolite composed of hematite and quartz or chlorite may sometimes be observed (Plate 4.10 (b)).

Iron oxides occur as fine grains, typically less than 1 mm in size, within the chloritic mass and are marked in thin section by the darkened haloes around grains (Plates 4.10 (c)-(d)). These haloes are considered to represent radiation damage caused by fine (U-Th)-bearing REE minerals. This feature is supported by significant coincident radiometric anomaly highs over the orebodies.

Sulphide mineralisation is dominated by pyrite with considerable amounts of chalcopyrite developed in places and lesser amounts of bornite, arsenopyrite and molybdenite (Crocker *et al*., 2001). Pyrite occurs as heavily-pitted, euhedral, pyritohedral crystals (Plates 4.10 (e)-(f)) or as subhedral and fragmented grains, and ranges in size from ~10 mm to 1 mm or less. Pyrite appears to be paragenetically predated by magnetite, chalcopyrite and fluorite (Plates 4.11 (a)-(b)), and is commonly enclosed by coarse fluorite (Plate 4.11 (c)).

Chalcopyrite is the dominant copper-bearing mineral and usually occurs in close association with pyrite. It forms wispy and irregularly-shaped grains that occur within pyrite and fluorite or on their own (Plates 4.11 (d)-(f)).

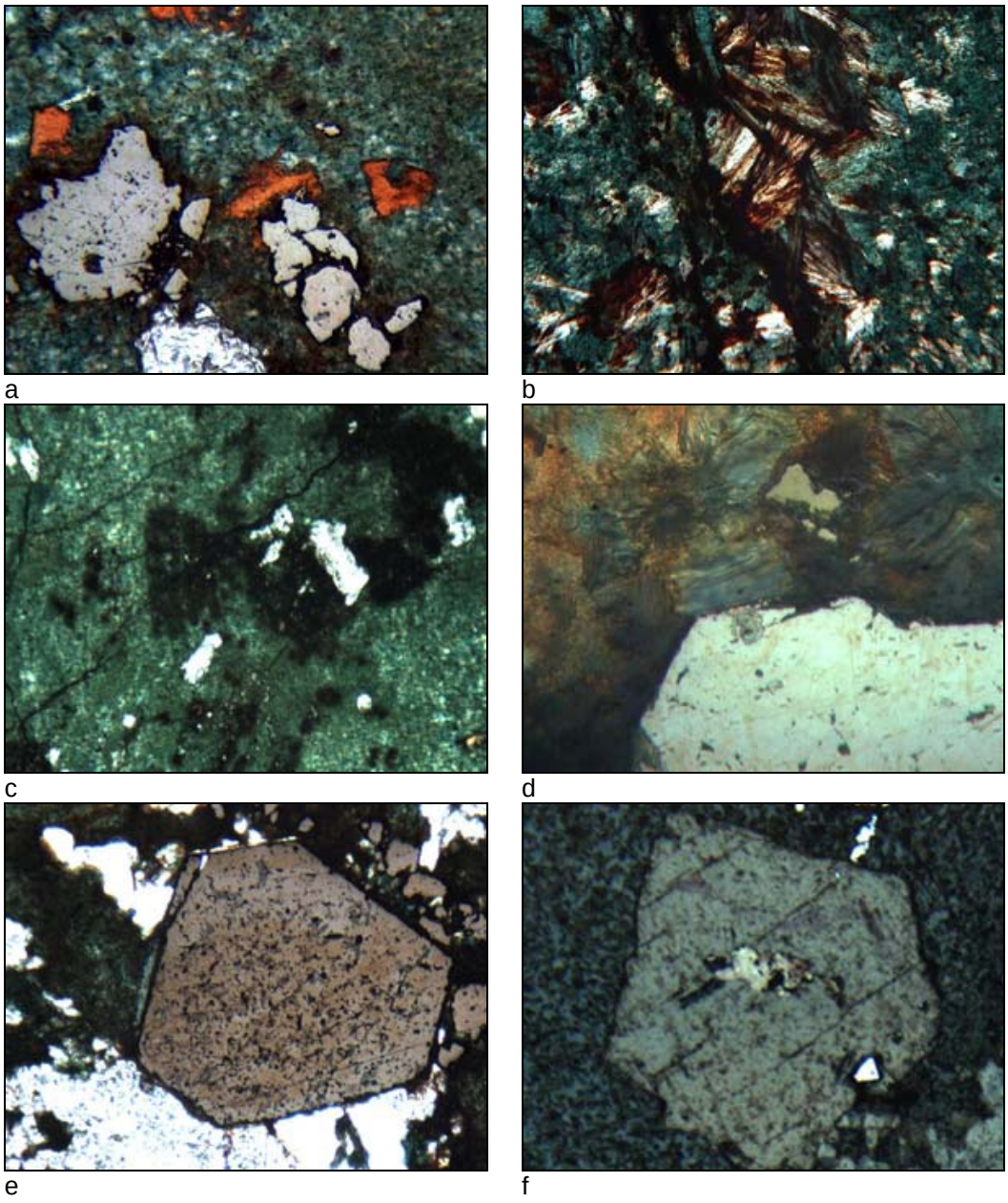

Plate 4.10. a) Chlorite-specularite-fluorite ore of Ruigtepoort Mine with fragmented pyrite grains and bright red iron oxides. Reflected with Plane polars x10; field of view is 0.85 mm; Photo ID: 11001-ZG. b) Chlorite and ferrohydroxides after actinolite in radiating growths. Plane polars x20; field of view is 0.45 mm; Photo ID: 11611-D. c) Chlorite groundmass with fluorite and minor sulphides. Black spots are radiation damage around thorium-rich minerals. Reflected with Plane polars x4; field of view is 2.75 mm; Photo ID: 11001-R. d) Iron oxide staining within the chlorite groundmass. Euhedral pyrite grain in bottom field of view with small pyrite grains above. Reflected with Plane polars x80; field of view is 0.10 mm; Photo ID: 11001-ZC. e) Heavily-pitted, euhedral pyrite crystal with pyritohedral habit; predates fluorite and chlorite. Reflected with Plane polars x4; field of view is 2.75 mm; Photo ID: 11001-E. f) Pyritohedral pyrite with chalcopyrite core and small angular fluorite inclusion. Fine exsolution-type lamellae unidentified. Reflected with Plane polars x4; field of view is 2.75 mm; Photo ID: 11001-X.

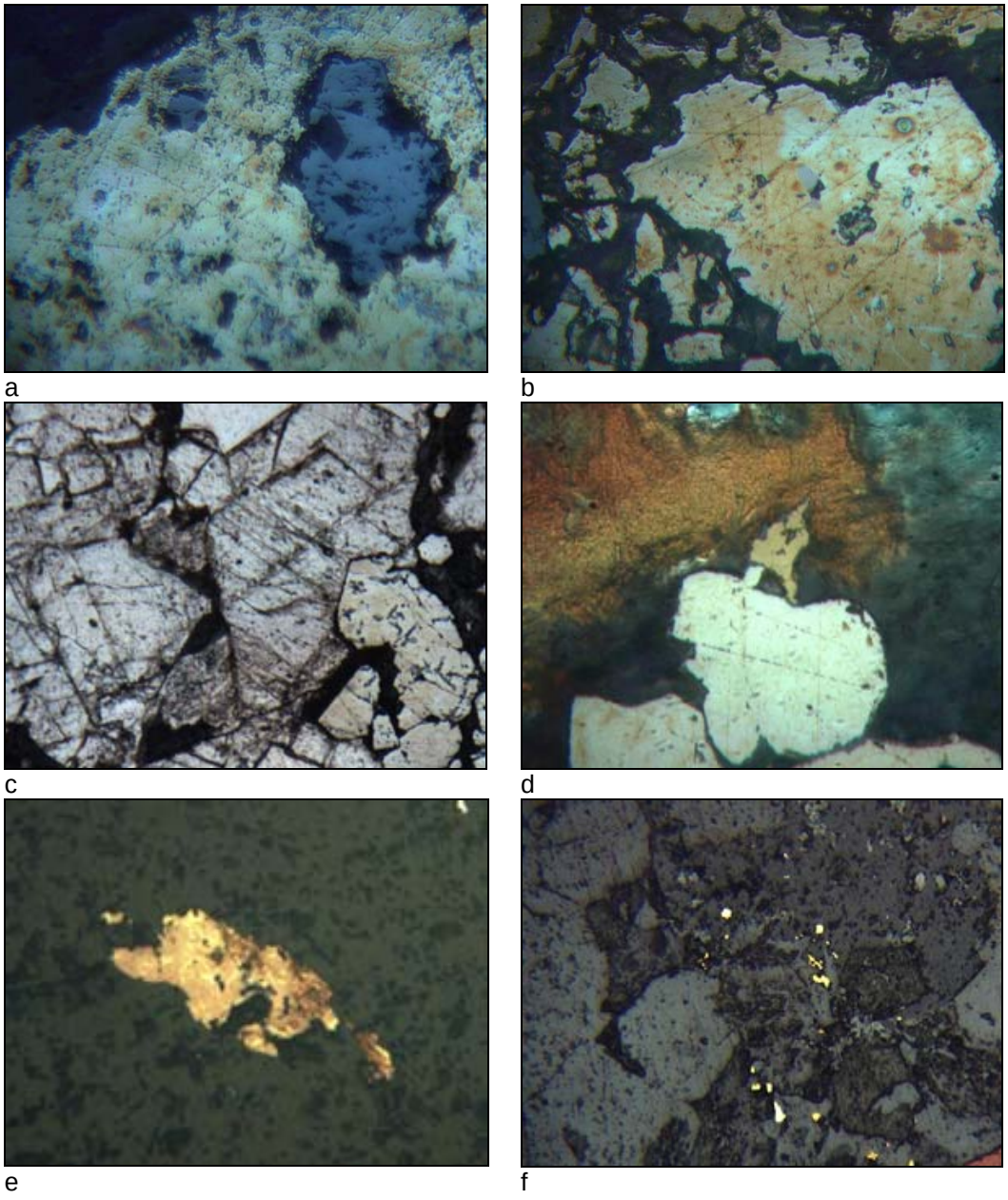

Plate 4.11. a) Inclusions in pyrite of earlier-formed ore phases magnetite. Reflected x40; field of view is 0.20 mm; Photo ID: 11160-T. b) Inclusions in pyrite of earlier-formed ore phase, possibly ilmenite. Reflected x80; field of view is 0.10 mm; Photo ID: 11160-J. c) Sub-euhedral pyrite enclosed by later-formed fluorite. Reflected with Plane polars x4; field of view is 2.75 mm; Photo ID: 11001-G. d) Pyrite with flame-like chalcopyrite in chlorite-iron oxide groundmass. Reflected with Plane polars x80; field of view is 0.10 mm; Photo ID: 11001-ZF. e) Chalcopyrite with reddish brown alteration/exsolution in pyrite. Reflected with Plane polars x20; field of view is 0.45 mm; Photo ID: 11001-U. f) Fine chalcopyrite and pyrite fragments in coarse fluorite. Reflected with Plane polars x10; field of view is 0.85 mm; Photo ID: 11002-C.

Silicified Core Assemblage

The core assemblage found at Ruigtepoort Mine is apparently a consequence of metasomatic replacement of the chlorite rock involving intense silicification and sulphidation. These fluids must have been extremely oxidising and metal charged. The resultant assemblage consists of highly-included, mosaic-textured quartz with considerable overgrowth rims (Plate 4.12 (a)-(b)). The quartz grains are noted as having sweeping extinction and terminating in triple junctions.

The other principal phase is highly-fractured sulphides exhibiting acicular habits; dominated by pyrite with associated arsenopyrite and trace chalcopyrite and molybdenite. Pyrite occurs as highly-pitted, highly-fragmented accumulations of presumably once euhedral forms, which are preserved in only a few instances, set in a siliceous frame (Plate 4.12 (c)). Arsenopyrite is a prominent component of the sulphide assemblage and is likely related to fluids responsible for gold mobilisation (Plate 4.12 (d)).

Purple and colourless fluorite, occurring within the quartz, apparently predates the metasomatism and is considered to be a remnant phase of the pre-existing chlorite-specularite-fluorite assemblage.

Anomalous gold contents have been reported for samples of this assemblage. Gold occurs as minute grains in quartz (Plates 4.12 (e)-(f)).

The epithermal nature of this rock has not been determined by either fluid studies or otherwise, and is merely a qualitative representation of the characteristics of the rock as a whole.

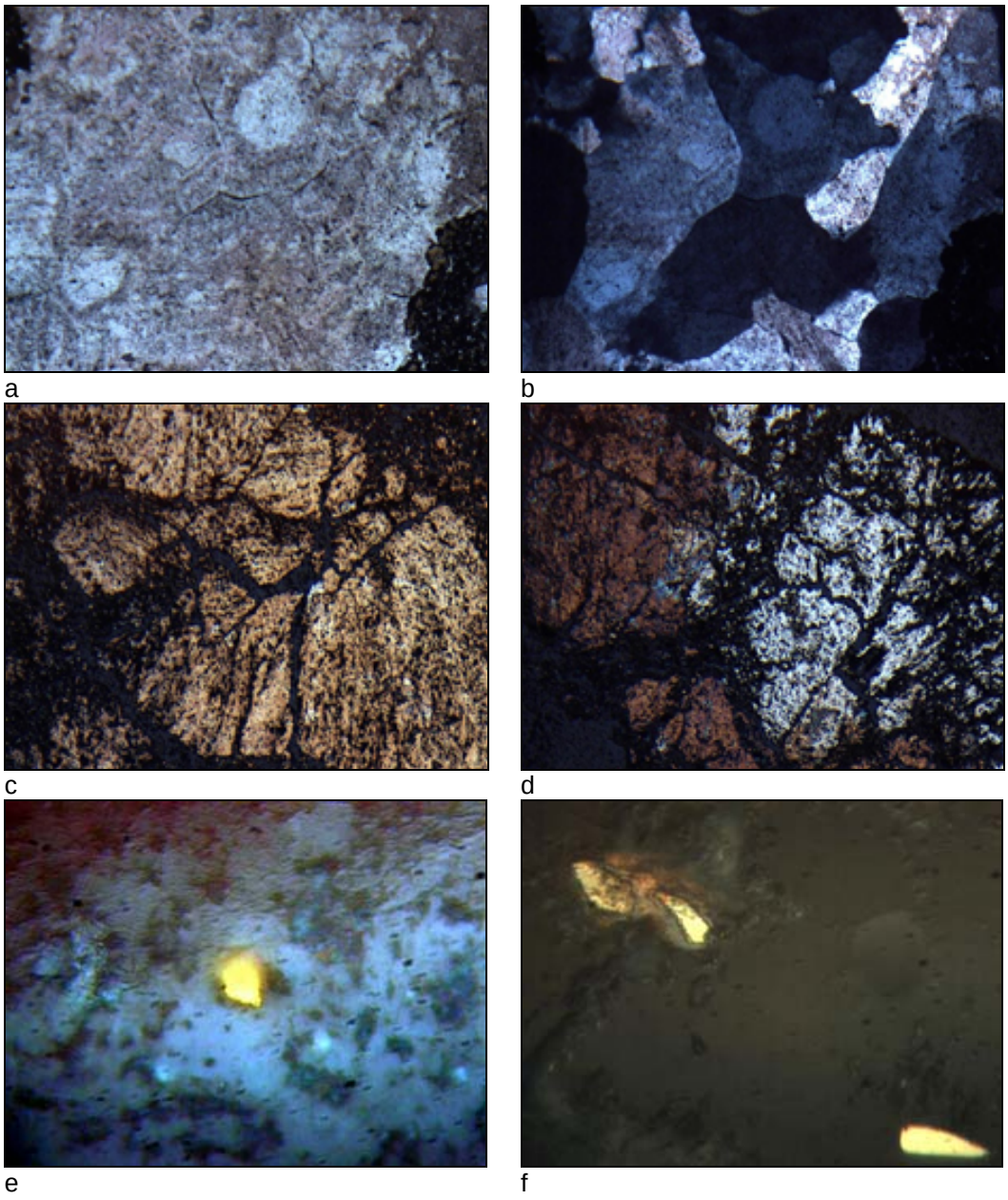

Plate 4.12. a) Multiple growth quartz of sinter. Plane polars x4; field of view is 2.75 mm; Photo ID: 11159-E. b) Mosaic textured epithermal quartz. Crossed polars x4; field of view is 2.75 mm; Photo ID: 11159-D. c) Highly-pitted and fractured pyrite grain. Reflected light x4; field of view is 2.75 mm; Photo ID: 11159-A. d) Highly-fragmented arsenopyrite and pyrite. Reflected light x4; field of view is 2.75 mm; Photo ID: 11159-B. e) Gold grain in quartz 0.01 mm (10 μ) in size. Reflected light x80; field of view is 0.10 mm; Photo ID: 11160-ZT. f) Multiple gold grains in quartz approximately 0.015 mm (15 μ) in length. Reflected light x80; field of view is 0.10 mm; Photo ID: 11001-Y.

REE-enriched Sediments

The xenolithic sediments that become increasingly more common towards the roof of the granite sheet retain many characteristics of the supposed Transvaal Supergroup orthoquartzitic precursor. In general, they consist of tightly packed, and for the most part recrystallised, irregularly-shaped quartz grains with minor iron oxides and sericite (Plate 4.13 (a)).

In mineralised samples of this rock, hematite, which may be specularitic, forms a significant component of the total rock and encloses quartz grains or occurs along grain boundaries (Plate 4.13 (b)). It is considered that portions of the original assemblage which may have comprised nearly 99 % quartz, must have been leached out in order to make space for hematite. In many samples, the iron content may account for 20 % or more of the total rock. In reflected light, hematite can be seen to occur as a netted mass with small inclusions of remnant quartz grains (Plate 4.13 (c)).

The presence of rare earth minerals forms an important signature for mineralisation associated with the sedimentary xenoliths, with up to ~1 % Ce and ~0.4 % Y as maximum reported values for these rocks. According to Crocker *et al*. (2001), the most important rare earth minerals may be britholite, such as at the Blokspruit prospects, and bastnaesite, such as at Slipfontein Fluorspar Mine. Bastnaesite ($(Ce,Y,La)(CO_3)F$) within the sedimentary xenolith occurrences occurs as high relief, granular grains with an uneven fracture and may be ~0.20 mm in size (Plate 4.13 (d)).

Sericite is an accessory phase to the assemblage and generally occurs in clotted masses and is likely a late-formed phase (Plate 4.13 (e)-(f)).

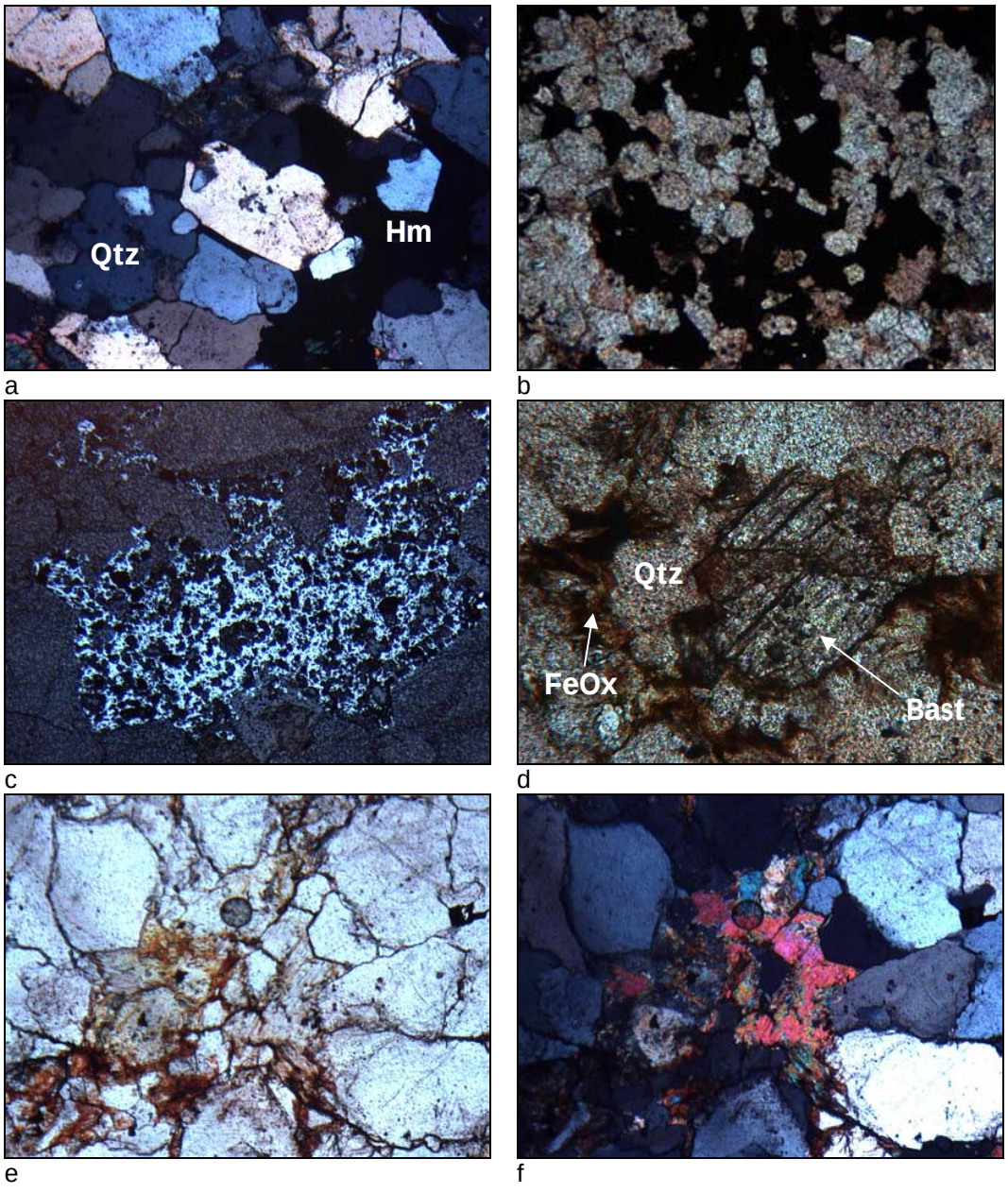

Plate 4.13. a) Tightly packed metaquartzitic rock with interstitial hematite. Small quartz grains included in larger grains (centre left) evidence for recrystallisation. Qtz=quartz, Hm=hematite. Crossed polars x4; field of view is 2.75 mm; Photo ID: 11150-D. b) Quartzitic xenolith where 40-50 % of field of view is replacement hematite. Plane polars x4; field of view is 2.75 mm; Photo ID: 11087-C. c) Specularitic hematite replacement in sedimentary xenolith. Reflected light x4; field of view is 2.75 mm; Photo ID: 11150-E. d) High-relief rare earth mineral bastnaesite. Qtz=quartz, FeOx=iron oxide, Bast=bastnaesite. Plane polars x20; field of view is 0.45 mm; Photo ID: 11087-E. e) Sericite clot in sedimentary xenolith. Plane polars x4; field of view is 2.75 mm; Photo ID: 11150-F. f) High birefringence of sericite clot in sedimentary xenolith. Crossed polars x4; field of view is 2.75 mm; Photo ID: 11150-G.

4.3. Alteration Assemblages & Temporal Relations to the Mineralising Event

The passage of fluid through rock may be marked by the presence of veining, usually of a silicic or carbonate composition, and the presence of alteration, which reflects the composition of the fluid and the original host rock, the temperature and pressure conditions and the changing fluid/rock ratio. The presence of hydrothermal alteration may be used as a useful guide for mineral exploration and the nature of the alteration indicative of the style and composition of the expected ore assemblages. Typical compositional changes caused by various common alteration processes are introduced in Table 4.1.

IOCG deposits are generally associated with sodic-potassic, potassic or hydrolytic alteration, and the style and intensity of alteration is affected by the degree of interaction between magmatic fluids and meteoric or connate fluids. Other factors affecting the resultant alteration around IOCG mineralisation are the host lithology composition and the depth of formation. In general, sodic alteration forms at deeper levels (2-3 km) and may extend over 10-100s km^2 from the ore zone. This evolves towards potassic alteration at intermediate levels including K-metasomatism and sericitisation, and hydrolytic alteration at shallow levels involving sericitisation and silicification. Intense Fe-metasomatism is prevalent locally in host rocks.

Table 4.1. Effects of Secondary alteration of granites (after Stemprok & Skvor, 1974).

Albitisation	- K-feldspar - Ca plagioclase + albite	+ Na_2O - K_2O
Muscovitisation	- K-feldspar - plagioclase - biotite + muscovite	- K_2O
Greisenisation	- K-feldspar - plagioclase - biotite + quartz + mica	- Na_2O + SiO_2 + Al_2O_3
Silicification	- K-feldspar - biotite	+ SiO_2
Sericitisation	- K-feldspar - plagioclase	+ K_2O CaO
Kaolinisation	- K-feldspar - plagioclase	- Na_2O - K_2O

Complex paragenetic assemblages may be developed due to complications arising from multiple alteration events that overprint earlier assemblages. These multiple events may represent responses to changing fluid compositions and/or pressure-temperature conditions or may represent fluids derived from subsequent magmatic episodes.

Below is a brief description of the salient styles of alteration observed in this study, and some ideas on how they may have influenced mineral assemblages, mineral paragenesis and the development of ore mineralisation.

Deuteric

Deuteric alteration encountered in the study area is perceived to be a typical late-magmatic effect with cooling and consolidation of the magma (i.e. 600-750 °C). It is characterised by reddening of the K-feldspars caused by the incorporation of iron-oxyhydroxides within the feldspar lattices and chloritisation of magmatic mafic phases such as biotite and hornblende (Plates 4.14 (a)-(b)). These effects were enhanced as the granite sheet continued to fractionate and are most prevalent in the late-derivative granites such as the Klipkloof granite, Bobbejaankop granite and Nebo granites in the upper portions of the sheet.

Sodic (±Calcic) Alteration

Sodic (±calcic) alteration has been shown to be a likely contributing process to the development of both barren and mineralised ironstones in IOCG districts (Oliver *et al*., 2004). This alteration tends to be regional scale and responsible for the liberation of iron and potassium from affected country rocks. It may be possible to exsolve the necessary (CO_2-rich) brines from crystallising felsic magmas to produce the ore-forming constituents with the capacity for regional sodic alteration (Cline & Bodnar, 1991; Marschik & Fontboté, 2001).

The formation of metasomatic ironstones involves most of the same elements lost during albitisation; i.e. Fe, K, Ba, Rb ± Ca, Sr, Co, V, Mn, Pb, and Zn (Oliver *et al*., 2004). It is unlikely that sodic alteration would have any effect on the significant mass transfer of Cu, but the effects of the alteration may represent an unrelated but perhaps necessary precursor condition, with subsequent Cu-bearing brines interacting with earlier ironstones.

Albitisation is by way of the simple alkali earth exchange reaction shown below:

(4-1) $\underset{\text{K-feldspar}}{KAlSi_3O_8} + Na^+_{(aq)} \leftrightarrow \underset{\text{Albite}}{NaAlSi_3O_8} + K^+_{(aq)}$

From the forward reaction (4-1) above, it can be seen that with albitisation of the K-feldspar K^+ ions are liberated. Freeman (1998) noted that a further effect is the release of iron from the feldspar lattice which may be deposited along cleavage planes or migrated elsewhere.

The Na-K activity-activity diagram after Oliver *et al*. (2004) in Figure 4.1 models the highly-saline fluids in equilibrium with a two-feldspar granitoids and its effect on surrounding calc-silicate country rocks. During albitisation, the Na^+/H^+ ratio is shown to shift towards the K-feldspar boundary as potassium is liberated, increasing the K-metasomatism potential downstream. At the point that K^+ activity may be too low to produce K-metasomatism, sericitisation may take over. The modelled products of alteration are presented in Figure 4.2 as a function of the changing fluid/rock ratio but may or may not necessarily be relevant to discussions on alteration of felsic country rocks.

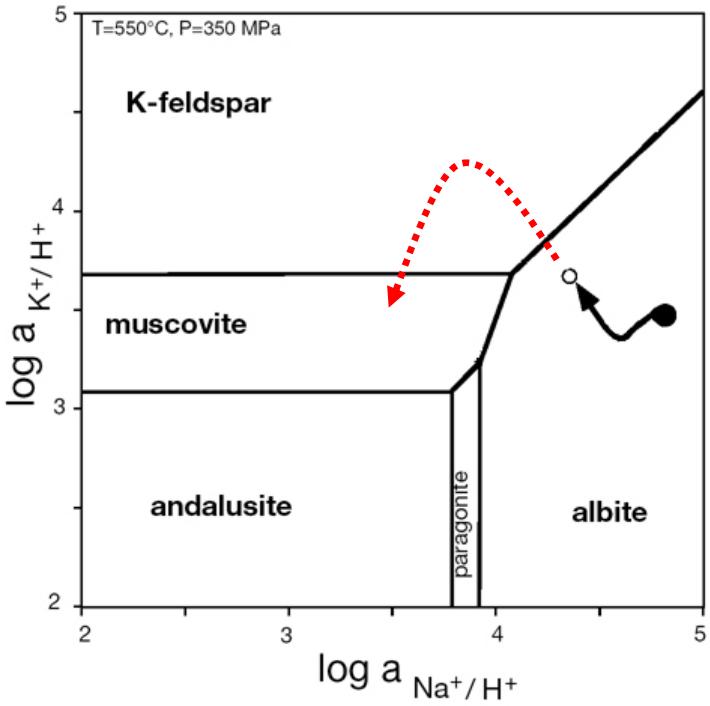

Figure 4.1. Na-K activity-activity diagram, constructed for the P-T condition indicated. The starting fluid is marked by the closed black dot derived from fluid inclusion data for Mount Angeley two-feldspar quartz monzonite. The open circle represents the fluid after albitisation of calc-silicate country rocks with the solid arrow tracing the path of intermediate experimentally derived results. Dotted lines trace hypothetical path of projected fluid evolution producing corresponding K-metasomatism and sericitisation (after Oliver *et al*. 2004).

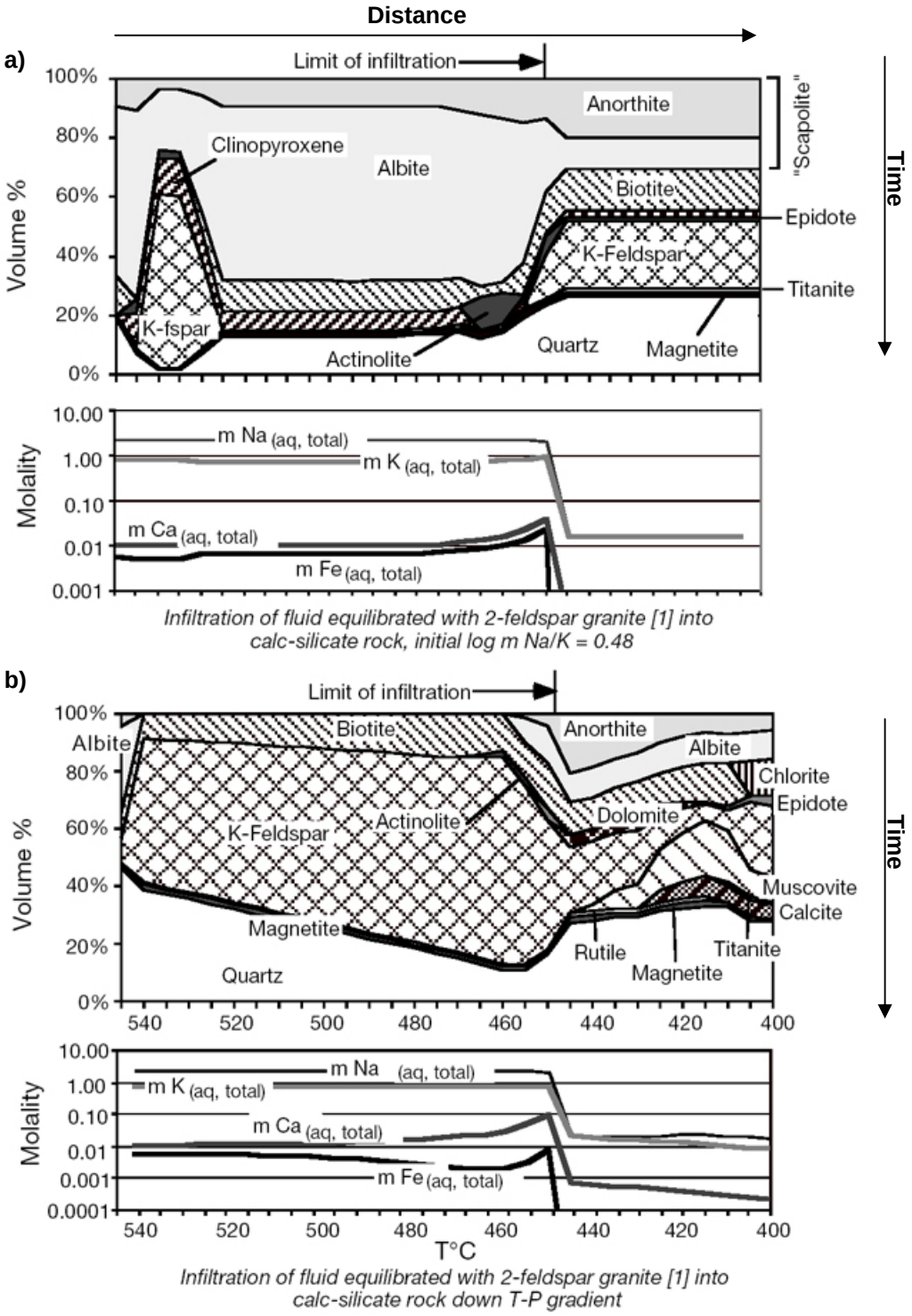

Figure 4.2. Models by Oliver *et al.* (2004) portraying progressive infiltration of fluids through a rock column. Fluid of the same composition is added from the left and allowed to react. On completion of each reaction step (ticks on x-axis) the fluid is displaced to the next block of rock and new fluid added as before. The bottom portion of each diagram shows the calculated molalities of the indicated fluid species. a) Isothermal infiltration of calc-silicate rock with conditions as indicated. b) Retrograde (down P-T) infiltration of calc-silicate rocks from 550°C and 350 MPa to 400°C and 200 MPa (after Oliver *et al*., 2004).

Potassic Alteration / K^+- Metasomatism

The post-magmatic processes associated with K-metasomatism/potassic alteration include: (1) base-exchange reactions in feldspars, specifically Na for K, or, K for Na; (2) changes in the structural state of feldspars; (3) albitisation (discussed above); (4) microclinisation; and (5) growth of tri-octahedral micas; i.e. Fe^{3+}- and Al^{3+}-dominated (Pirajno, 1992) (see Plates 4.14 (c)-(e)). The products and characteristics of each of these processes may be significantly different, and any or none may accompany another process depending on various conditions. Potassium metasomatism is characteristically associated with the replacement of feldspar and quartz by K-feldspar (microclinisation) or to a lesser degree albite (albitisation). Biotite is another important product of potassic alteration (Plate 4.14 (f)). Minor phases that may form along with the K-feldspar and biotite include sericite, chlorite and quartz with accessory amounts of magnetite, hematite and anhydrite.

With progressive microclinisation, a nett desilicification of the granitic assemblage may result in the formation of episyenites such that quartz and mafic phases are replaced entirely by feldspar.

The presence of potassic alteration in the high-temperature cores of porphyry and epithermal mineralising systems is well documented, with assemblages of K-feldspar-biotite-quartz, K-feldspar-chlorite, K-feldspar-biotite-magnetite, with possible accessory phases of albite, sericite, anhydrite, apatite, and occasionally rutile (Pirajno, 1992), being common. In IOCG environs, potassic alteration comprises a significant component of the alteration halo and usually develops at an intermediate level in the system. It typically develops in 400-600 °C range corresponding to hydrothermal fluids.

Burnham & Ohmoto (1980) modelled the alteration developed by aqueous chloride solutions derived from a high-temperature magmatic source (Figure 4.3). Initial fluids may become enriched in KCl relative to NaCl and HCl if they are

able to equilibrate with the hornblende-bearing magma and even more enriched if they are subsequently able to equilibrate with the biotite-bearing component. As these fluids cool, the resultant alteration is initially one dominated by the ionic exchange of potassium with sodium and calcium, principally in feldspar and biotite; to produce potassic alteration. These exchange reactions gradually lower the KCl/HCl ratio in the aqueous phase, which ultimately enters into the stability field of muscovite to produce sericitic alteration principally in the K-feldspar component. Further cooling causes the KCl/HCl ratio to increase as K-feldspar is converted to sericite and quartz.

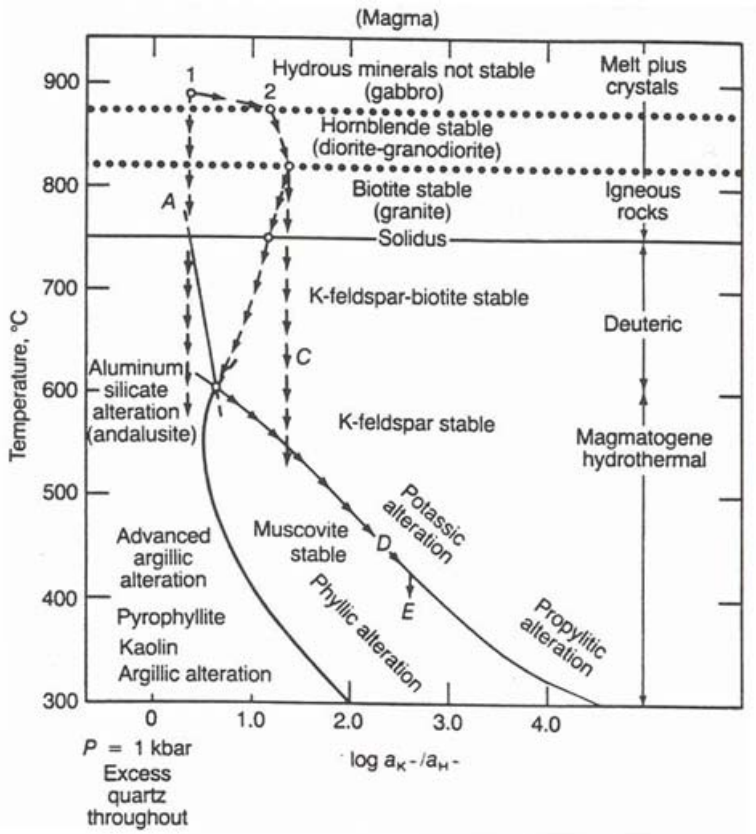

Figure 4.3. Plot of log a_{K+}/a_{H+} vs. temperature at 1 kb showing the temperature ranges of alteration assemblages associated with mineralisation. Point 1 marks the original fluid. Point 2 marks the position of the fluid equilibrated with the hornblende-bearing magma. Various paths may be taken by the fluid on cooling with deuteric alteration being followed by potassic alteration and phyllic alteration (after Burnham & Ohmoto, 1980).

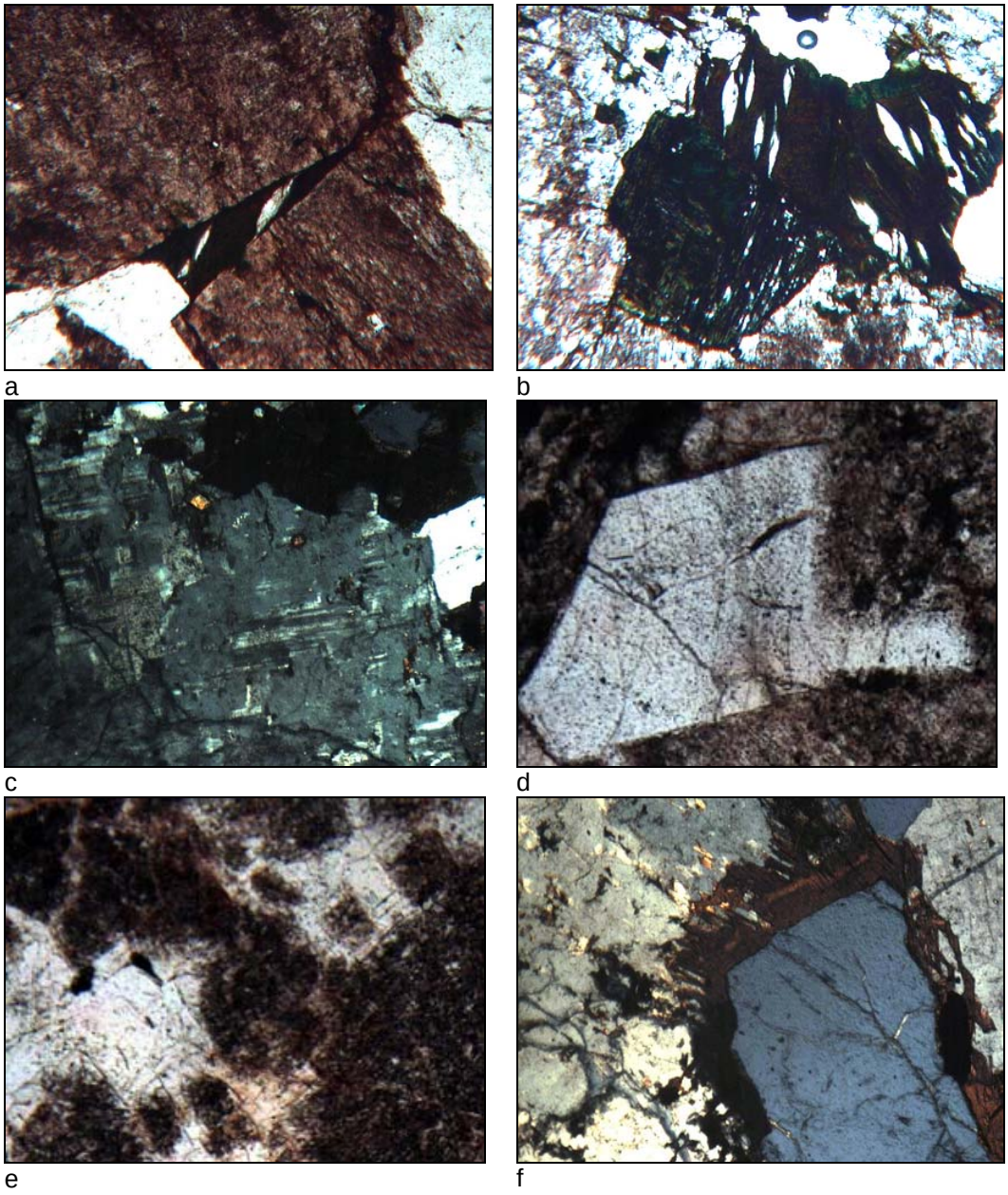

Plate 4.14. a) Deuterically altered, reddened K-feldspar with interstitial symplectic biotite. Plane polars x4; field of view is 2.75 mm; Photo ID: 11023-G. b) Deuteric chloritised symplectic biotite. Plane polars x4; field of view is 2.75 mm; Photo ID: 11023-I. c) Microclinisation of albite feldspar. Crossed polars x4; field of view is 2.75 mm; Photo ID: 11120-D. d) Microclinisation of granite; new K-feldspar growth at the expense of quartz. Plane polars x4; field of view is 2.75 mm; Photo ID: 11004-J. e) Microclinisation of granite; new K-feldspar growth at the expense of quartz. Plane polars x4; field of view is 2.75 mm; Photo ID: 11177-B. f) Growth of secondary biotite related to K-metasomatism; growing at expense of pre-existing feldspar. Crossed polars x4; field of view is 2.75 mm; Photo ID: 11120-H.

Sericitisation / H^+ Metasomatism / Hydrolysis

Hydrolysis, or hydrogen ion metasomatism, is an extremely important phenomenon of hydrothermal alteration involving the ionic decomposition of H_2O into H^+ and OH^- (Guilbert and Park, 1986; Pirajno, 1992). The ratio of H^+/OH^- changes during reactions with silicate minerals, which affects the pH of interacting solutions and its cation solubility characteristics. H^+ ions may also be obtained from subsolidus reactions during alkali metasomatism or from acids in the hydrothermal solutions. A typical example of hydrogen ion metasomatism, or hydrolytic decomposition of feldspar, is given by:

$$(4\text{-}2)\quad \underset{\text{K-feldspar}}{3KAlSi_3O_8} + 2H^+ \leftrightarrow \underset{\text{muscovite}}{KAl_3Si_3O_{10}(OH)_2} + \underset{\text{quartz}}{6SiO_2} + 2K^+$$

In terms of this reaction, the hydrolysis of K-feldspar to muscovite is isochemical; requiring only the presence of H^+ ions in an aqueous solution. The formation of muscovite or sericite from the hydrolysis of feldspars, i.e. *sericitisation*, forms over a range of temperatures, and is associated with mesothermal precious metal ores, as well as porphyry Cu ores and volcanogenic massive sulphide deposits in felsic rocks (see Plates 4.15 (a)-(f)).

It can be seen from the equation that the products of this reaction include quartz and K^+ ions in aqueous solution which in an open system may be migrated and enhance K-metasomatism and silicification effects elsewhere. The reaction above is a simplification of what may occur and it is likely that actual hydrolytic reactions would be influenced by cations in solution derived from other reactions and sources, which in turn would complicate and resultant assemblage.

The distribution of sericitic alteration may yield indications of the proximity to ore mineralisation. In general, sericitic alteration forms under decreasing temperatures and is more distal than other associated cogenetic styles of alteration.

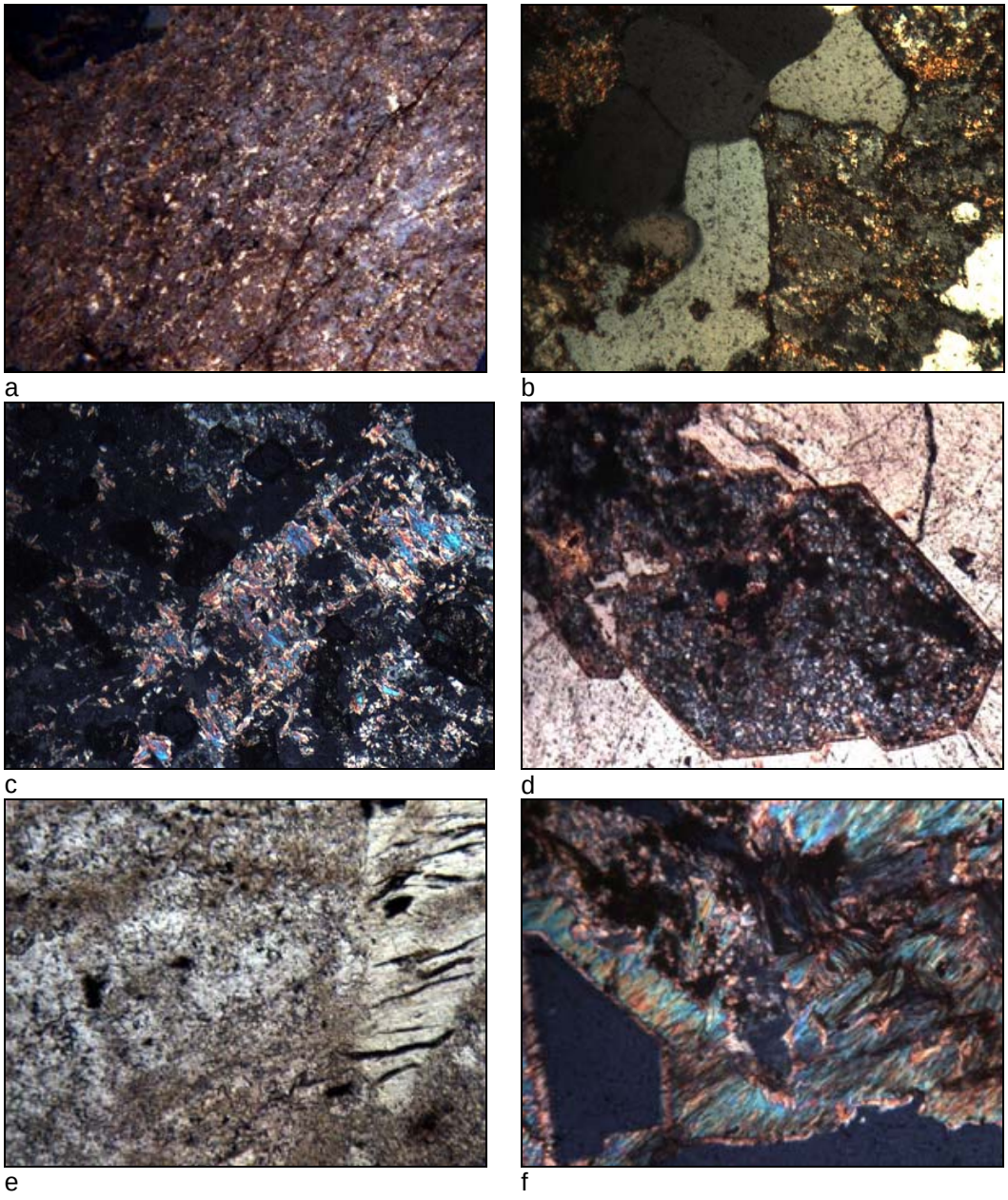

Plate 4.15. a) Sericite replacement of perthite K-feldspar. Crossed polars x4; field of view is 2.75 mm; Photo ID: 11125-B. b) Sericitisation of K-feldspar; quartz grains unaffected. Crossed polars x10; field of view is 0.85 mm; Photo ID: 11115-A. c) Near-complete replacement of K-feldspar in intensely altered zone. Crossed polars x4; field of view is 2.75 mm; Photo ID: 11078-D. d) Intensely sericitised K-feldspar exhibiting primary crystal habit; associated quartz and hematite. Crossed polars x4; field of view is 2.75 mm; Photo ID: 11201-E. e) Intensely sericitised granite; biotite replaced by muscovite with magnetite symplectic banding still apparent. Plane polars x10; field of view is 0.85 mm; Photo ID: 11111-D. f) Intense muscovite replacement of feldspars with associated iron oxides, possibly liberated from feldspar with alteration. Crossed polars x4; field of view is 2.75 mm; Photo ID: 11078-F.

Silicification

Silicification in country rocks and host assemblages commonly accompanies other styles of alteration or is a by-product of metasomatism, as in the isochemical hydrolysis of feldspar shown by reaction (4-2). Quartz may be precipitated locally in available pore spaces or along grain boundaries (Plate 4.16 (a)) or transported to other sites within the system.

The majority of fractures that carry fluid are at least partially filled with quartz. Quartz may be retained by fluids and is commonly a late-stage, low temperature precipitate.

Silicification of actinolite is common in some of the examined deposits and is accompanied by abundant hematite and fluorite. This may be expressed by the following equation:

(4-3) $\underset{\text{Ferroactinolite}}{Ca_2Fe^{2+}{}_5Si_8O_{22}(OH)_2} + 2F^+ + 8H_2O \rightarrow \underset{\text{Hematite}}{5Fe_2O_3} + \underset{\text{Quartz}}{8SiO_2} + \underset{\text{Fluorite}}{2CaF_2} + 18H^+$

Production of abundant H^+ has the effect of making the residual hydrothermal fluid more acidic during progressive alteration.

Intense silicification, as developed in the core assemblage, involves the cation exchange of Si^{4+} in solution is added to the system. The core assemblage as observed at Ruigtepoort mine is thought to have been derived from precursor actinolite-chlorite-magnetite-quartz-fluorite assemblages. The final assemblage does not resemble the original at all and consists of quartz-sulphide-fluorite (Plate 4.16 (b)) and would have required the complete cationic replacement of most ionic species.

Chloritisation

Alkali earth metasomatism is achieved by cation base-exchange reactions like many of the reactions previously discussed. Chloritisation is an ubiquitous expression of this kind of metasomatism and forms in a variety of styles and under differing conditions. It is most commonly associated with low-temperature metamorphism but may accompany a host of other alteration scenarios. Chloritisation of mineral phases such as biotite, amphibole and feldspar is common (Plates 4.16 (c)-(f)), the latter according to the following equation:

(4-4) $\underset{\text{K-feldspar}}{2KAlSi_3O_8} + 6.5Mg^{2+} \rightarrow \underset{\text{Chlorite}}{Mg_{6.5}(Si_3Al)O_{10}(OH)_8} + K^+ + 12H^+$

Below is an attempt to model the reaction that may more closely resemble the observed Fe-rich mineral phases:

(4-5) $\underset{\text{K-feldspar}}{2KAlSi_3O_8} + 3Fe^{2+} + 1.5Mg^{2+} + 0.5Fe^{3+} + 8H_2O \rightarrow$

$\underset{\text{Chamosite/Thuringite}}{(Fe^{2+})_3(Mg^{2+})_{1.5}(Al^{3+})(Fe^{3+})_{0.5}Si_3AlO_{12}(OH)_6} + 3SiO_2 + 2K^+ + 10H^+$

As determined by the above equations, the effects of these reactions include the intense acidification of the residual fluids, which in turn have implications for metal solubility and transport, in addition to the potential for silicification and K-metasomatism. The effect of abundant fluorite within the system has not been adequately considered.

Changes between biotite and chlorite are common, occurring in early deuteric alteration and in late hydrothermal alteration. This reaction is given by the following equation:

(4-6) $\underset{\text{Biotite}}{2K(Fe.Mg)_3AlSi_3O_{10}(OH)_2} + 4H^+ \leftrightarrow$

$\underset{\text{Chlorite}}{(Fe,Mg)_5Al_2Si_3O_{10}(OH)_8} + (Fe,Mg)^{2+} + 3SiO_2 + 2K^+$

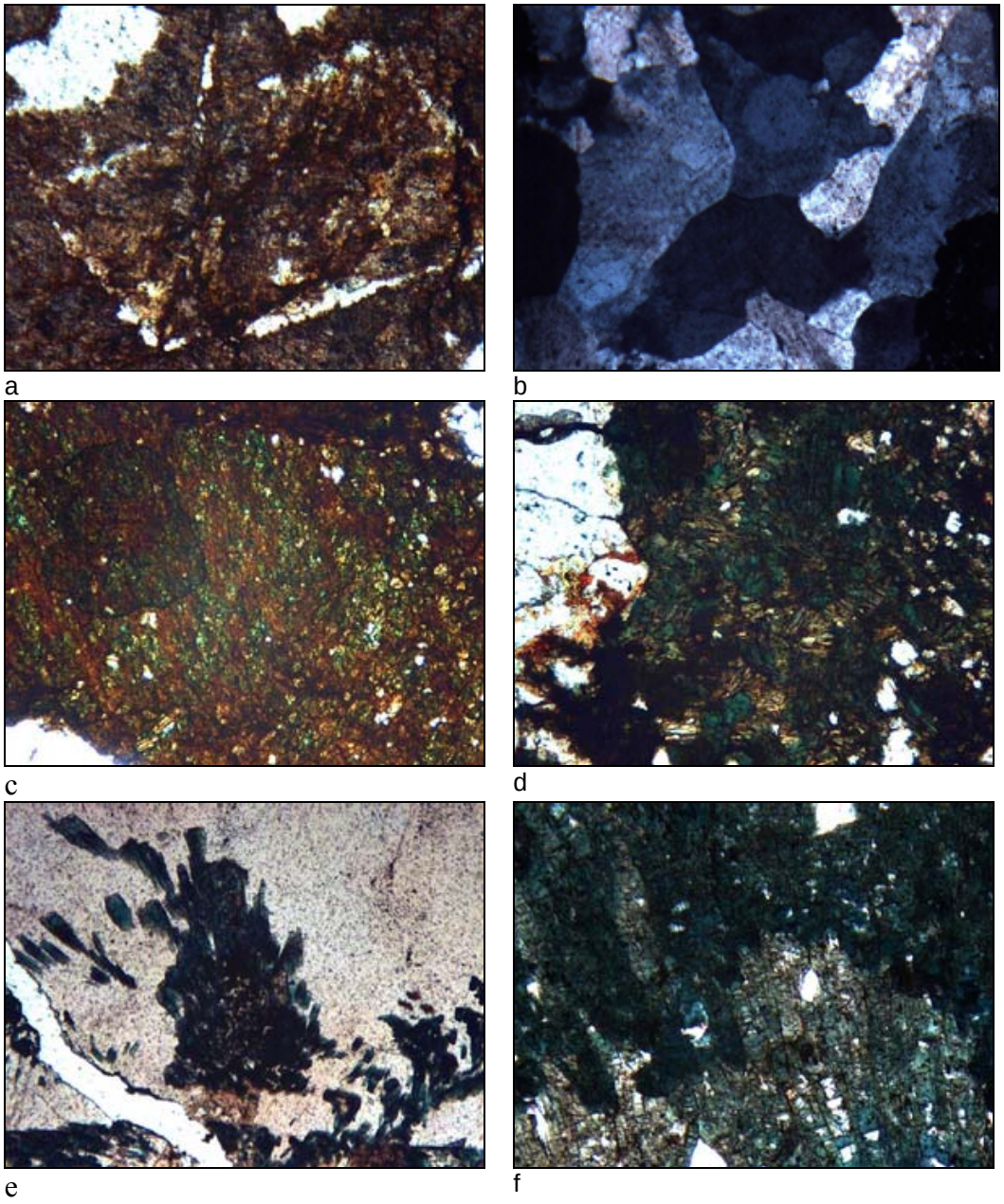

Plate 4.16. a) Quartz rim developed around K-feldspar grain likely derived from sericitisation. Abundant iron oxides. Plane polars x4; field of view is 2.75 mm; Photo ID: 11014-G. b) Epithermal sinter of Ruigtepoort mine where a quartz-sulphide assemblage has wholly replaced the original chlorite ore assemblage. Crossed polars x4; field of view is 2.75 mm; Photo ID: 11159-D. c) Intensely chloritised feldspar with iron oxide staining. Plane polars x4; field of view is 2.75 mm; Photo ID: 11066-B. d) Matted chlorite fans. Plane polars x4; field of view is 2.75 mm; Photo ID: 11067-F. e) Chlorite replacing quartz. Plane polars x4; field of view is 2.75 mm; Photo ID: 11059-A. f) Chlorite alteration of ferroactinolite. Plane polars x4; field of view is 2.75 mm; Photo ID: 11139-C.

Hematisation

Hematisation is generally considered as a transformation from magnetite to hematite corresponding to a redox reaction; that is to say that Fe^{2+} atoms in magnetite are oxidised to Fe^{3+}, as shown by equation:

(4-7) $2Fe_3O_4 + ½\ O_{2(g)} \rightarrow 3Fe_2O_3$
Magnetite Hematite

and inversely reduced,

(4-8) $3Fe_2O_3 + H_{2(g)} \rightarrow 2Fe_3O_4 + H_2O$
Hematite Magnetite

These equations may be relevant to Fe-conservative systems, such as those in the laboratory, but according to Ohmoto (2003), it may be possible to propagate the transformation in nonredox terms in natural systems that may well be open with respect to Fe. This may be particularly applicable in hydrothermal environments. The reversible reaction is achieved by the addition or leaching of Fe^{2+} atoms, without a change in valence of Fe or other atoms. This may be represented as follows:

(4-9) $Fe_3O_4 + 2H^+ \leftrightarrow Fe_2O_3 + Fe^{2+} + H_2O$ (Ohmoto, 2003)
Magnetite Hematite

This reaction may occur at any temperature, but like other acid-base reactions, it is favoured at higher temperatures (e.g. > 100 °C) where equilibrium may be more readily established. The equation indicates that an Fe^{2+} poor hydrothermal fluid could effect the transformation and liberate an Fe^{2+} ion (Figure 4.4).

Another consideration is the oxidation rate of pyrite, which is much faster than magnetite, such that if the transformation of magnetite to hematite had occurred by oxidation, it would follow that pyrite is also likely to be completely oxidised.

Hematisation of the granitic country rocks is represented by increased hematite

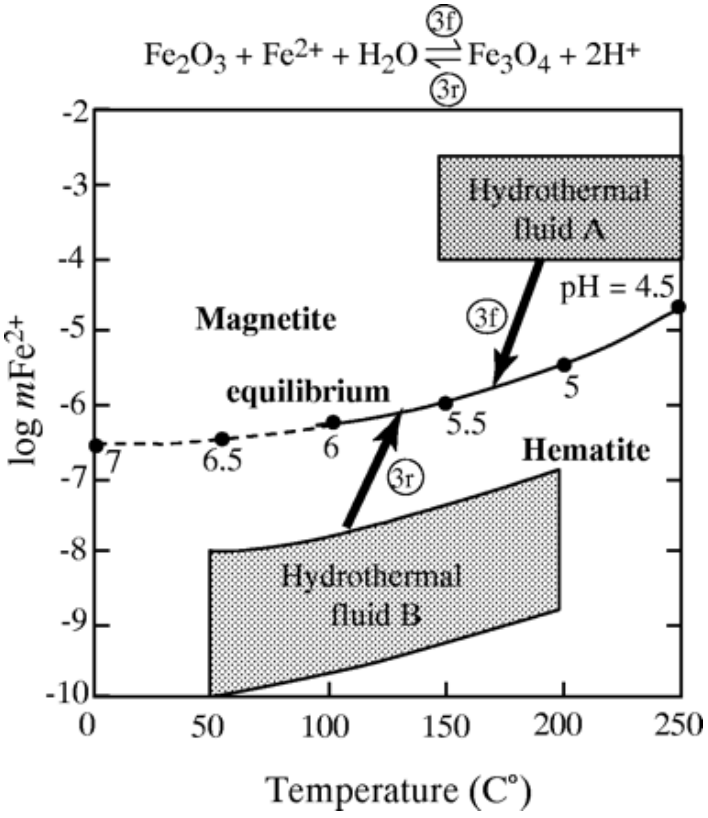

Figure 4.4. Comparisons of the Fe^{2+} contents of typical submarine hydrothermal fluids (A), typical subaerial geothermal fluids (B), and the fluids in equilibrium with the magnetite-hematite assemblage (solid and dashed line). The equilibrium Fe^{2+} values are estimated for the most common pH value of hydrothermal fluid at each temperature (cf. Ohmoto and Goldhaber, 1997). Note the reaction between hematite and hydrothermal fluid A will transform the hematite to magnetite (path 3f), whereas the reaction between magnetite and hydrothermal fluid B will transform the magnetite to hematite (path 3r). Taken from Ohmoto (2003).

and iron oxides in feldspars along perthite rims, within the grains, and as veinlets and stringers cross-cutting the perthites (Plate 4.17 (a)-(e)). Freeman (1998) noted that hematite and related iron oxides may be liberated from perthite lattices during albitisation and deposited in a similar fashion (Plate 4.17 (f)). It is presumed that a similar liberation of iron may be achieved during sericitisation, where feldspars are converted to sericite and quartz.

K-metasomatism of the granites may result in a similar effect with increased disordering of the feldspar lattice, which may make the granite more susceptible to alteration effects of subsequent sericitisation, hematisation or chloritisation, such that entire feldspars may be replaced.

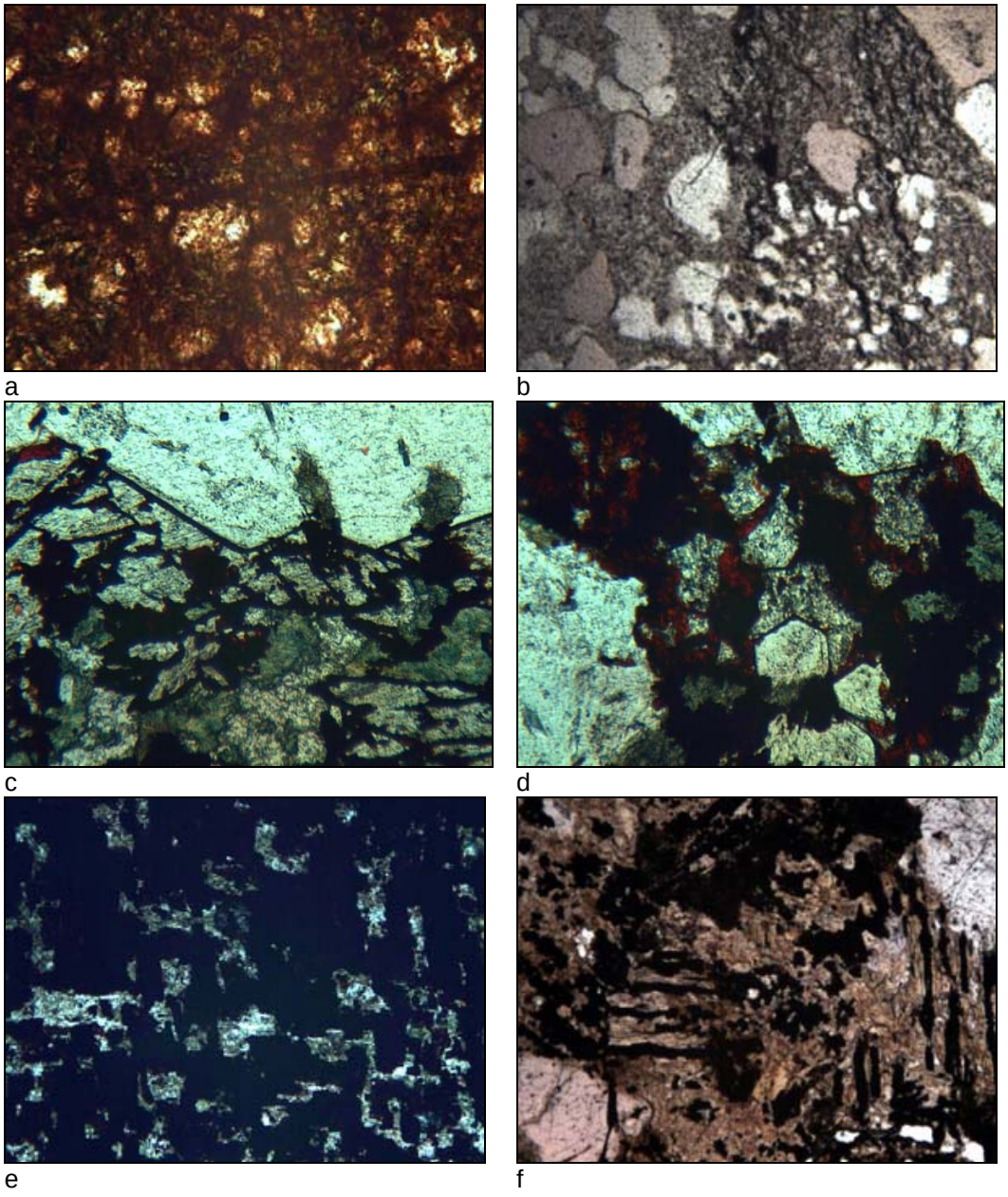

Plate 4.17. a) Hematisation of chloritised granites adjacent to Ruigtepoort mine; iron oxides distributed along fractures and between grains. Plane polars x20; field of view is 0.45 mm; Photo ID: 11066-E. b) Hematisation alteration front consisting of fine stringer veins of hematite in fine-grained granite. Left portion of photograph unaltered assemblage. Plane polars x4; field of view is 2.75 mm; Photo ID: 11187-D. c) Iron oxides precipitated along grain boundaries in chloritised granite. Plane polars x10; field of view is 0.85 mm; Photo ID: 11008-P. d) Iron oxides precipitated along grain boundaries. Plane polars x10; field of view is 0.85 mm; Photo ID: 11008-Q. e) Hematite precipitated in a patchwork pattern in coarse Bobbejaankop granite. Plane polars x4; field of view is 2.75 mm; Photo ID: 11068-C. f) Bands of hematite in intensely sericitised feldspar; may be consequence of iron liberation during alteration. Plane polars x4; field of view is 2.75 mm; Photo ID: 11082-A.

4.4. Paragenetic Sequence

Many of the paragenetic relationships observed in this study have been identified previously in discussions on alteration and mineralisation of the above section. The conclusions of these observations are illustrated in Table 4.2.

Depictions of the mineral paragenesis of IOCG systems generally place great emphasis on the iron oxidation state, usually an early magnetite stage followed by a hematite stage, or consider them solely as a function of changing temperature. It is apparent that these systems are far more dynamic than this and require consideration of factors including fluid composition, temperature, alteration, and iron oxidation state.

The changing nature of the fluids seems to be a critical component of these systems; evolving from an initial, highly-saline magmatic fluid to one with an increasingly greater connate or meteoric component. Alteration in the country rock reflects this fluid character and is an important consideration in the overall paragenesis. Mineralisation commonly occurs in the zone of mixing and is therefore also intrinsically related to alteration and fluid composition.

The early magmatic stage corresponds to high-temperature magmatic fluids (~600-750 °C) responsible for deuteric effects in the granites, dominated by perthitisation of K-feldspar, chloritisation of hornblende or biotite, and fixing of fine hematite in the feldspar lattices.

The late magmatic stage is represented by a high-temperature magmatic fluid (~500-600 °C) with initial signs of mixing with connate fluids. Pneumatolytic growth of actinolite is thought to have taken place at this stage, accompanied by fluorite, magnetite, siderite, and rare earth minerals (Crocker *et al*. 1988; Freeman, 1998). Siderite-magnetite-quartz ores at Slipfontein mine and ferroactinolite-britholite-magnetite-fluorite assemblages at the Ysterkop prospects are considered to have formed at this stage. Albitisation of the granites is not as widespread as might be

Table 4.2. Generalised paragenetic sequence of Ruigtepoort mine and satellite occurrences, with dominant style of alteration.

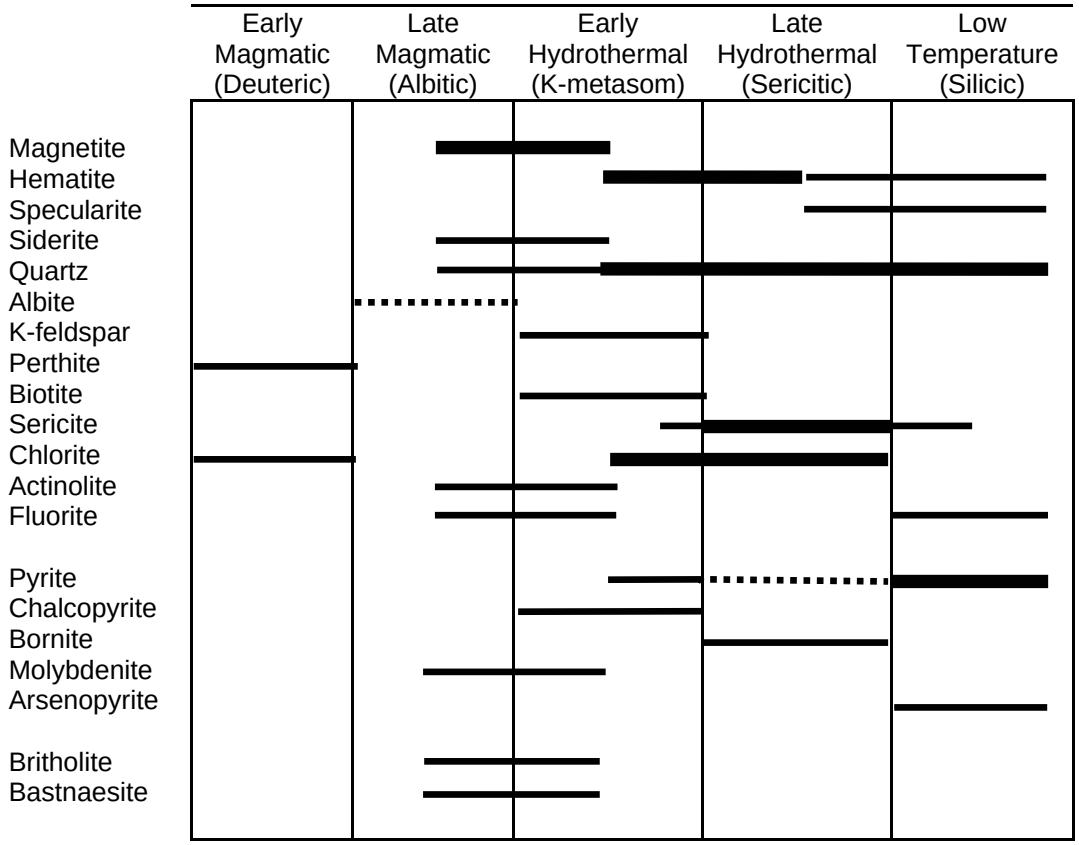

expected and few examples of new albite have been identified. Albitisation of K-feldspar may result in the exsolution of hematite from the crystal lattice.

The early hydrothermal stage corresponds to decreasing temperatures (~350-500 °C) and an increasing connate/meteoric fluid component, occurring at an intermediate depth. Alteration is characterised by K- and Fe- metasomatism with new K-feldspar and biotite developing, and magnetite forming in close association with biotite. At some point in this stage hematite becomes the dominant iron oxide phase. Sulphides associated with several of the deposits are thought to have developed at this time with intense chloritisation of host rocks.

The late hydrothermal stage (~250-400 °C) is dominated by intense sericitisation and silicification of country rocks and to a lesser extent ores. Continued oxidation of magnetite is expected.

The terminal stage corresponds to low-temperature effects (~50-200 °C) dominated by continued silicification and sulphidation of ores.

•••

This chapter described the principal rock types in terms of their petrography and characterised associated mineralisation. The alteration was examined and basic reaction equations were presented for the benefit of understanding chemical and volume changes related to the alteration. The next chapter will evaluate the assemblages and styles of alteration assessed in this chapter in terms of their geochemical characteristics and affinities to determine whether it is possible to track changes due to alteration chemically and to determine if it is possible to calculate relative volume changes in an affected rock.